Red light active Pt(IV)-BODIPY prodrug as a mitochondria and endoplasmic reticulum targeted chemo-PDT agent

Arpan Bera,[a] Srishti Gautam,[b] Somarupa Sahoo,[a] Apurba Kumar Pal,[a] Paturu Kondaiah,*[b] and Akhil R. Chakravarty*[a]

[a] *Department of Inorganic and Physical Chemistry, Indian Institute of Science, Sir C.V. Raman Avenue, Bangalore 560012, India. E-mail: arc@iisc.ac.in*

[b] *Department of Molecular Reproduction, Development and Genetics, Indian Institute of Science, Bangalore 560012, India. E-mail: paturu@iisc.ac.in*

Electronic Supplementary Information (ESI)

Table of contents

Figure S16. Unit cell packing diagram of **Me-L[1]**. Color codes: C, grey; H, white; O, red; B, yellow; F, lemon yellow; N, sky blue.

Figure S17. UV-vis spectra of the complex recorded at different concentrations in DMSO, and the absorbance was plotted against the concentration.

Figure S18. Fluorescence quantum yield for (a) rhodamine B in water (b) ligand **HL[1]** in DMSO.

Figure S19. Fluorescence quantum yield of complex **1** in DMSO.

Figure S20. Excited state lifetime of complex **1** in DMF.

Figure S21. Cyclic voltammogram of complex **1** in DMF containing 0.15 M TBAHFP (tetrabutylammonium hexaflurophosphate) at a scan rate of 50 mV/sec using glassy carbon as the working electrode. The split peaks are assignable to the irreversible two-electron transfer for Pt(IV)→Pt(II) and reversible response from the BODIPY moiety. The reverse anodic peak corresponds to only BODIPY oxidation.

Figure S22. Cyclic voltammogram of ligand **HL[1]** in DMF containing 0.15 M TBAHFP at a scan rate of 50 mV/sec using glassy carbon as the working electrode.

Figure S23. Time-dependent stability studies of complex **1** in 1:1 (v/v) DMSO/DPBS under dark condition.

Figure S24. Time-dependent stability studies of complex **1** at pH = 3 in 1:1 (v/v) DMSO/DPBS under dark condition.

Figure S25. Time-dependent stability studies of complex **1** at pH = 9 in 1:1 (v/v) DMSO/DPBS under dark condition.

Figure S26. Time-dependent stability studies of complex **1** at 4 mM GSH concentration in 1:1 (v/v) DMSO/DPBS under dark condition.

Figure S27. Confocal images of HeLa cells stained with IC_{50} concentration of complex **1** with increasing number of scans. A 633 nm laser with 6% output power was used for excitation, total experiment time was ~20 min.

Figure S28. Calibration curve for complex **1** in octanol for lipophilicity measurement.

Figure S29. Calibration curve for ligand in octanol for lipophilicity measurement.

Figure S30. Time-dependent ^{1}H NMR spectra of complex **1** irradiated with 642 nm laser. Intensity of 8.11 ppm peak gradually increased and 6.94 ppm peak for γ-proton of **HL[1]** gradually converted into a doublet.

Figure S31. (a) ESI-MS spectrum of complex **1** in solution (used for NMR study) after irradiating with 642 nm laser light. The 349.0359 peak is assignable to $[Pt(NH_3)_2Cl(DMSO\text{-}d_6)]^+$ and 627.2263 peak is due to free ligand released from the complex on light irradiation. (b) Isotopic distribution of $[Pt(NH_3)_2Cl(DMSO\text{-}d_6)]^+$ adduct with the inset showing simulated isotopic distribution.

Figure S32. Time-dependent ^{1}H NMR spectra of the complex **1** in presence of 5 equiv. ascorbic acid. The signal for six ammine protons (marked with red) disappeared due to metal reduction in presence of ascorbic acid as a reducing agent.

Figure S33. Changes in absorption spectra of DBBF containing ligand **HL[1]** (50:1 concentration ratio) on red light exposure (642 nm, 100 mW) in DMSO.

Figure S34. ΔOD vs. irradiation time for determining singlet oxygen quantum yield of complex **1** and **HL[1]** (MB, methylene blue as control).

Figure S35. (a) Gel diagram showing photocleavage of pUC19 DNA in presence of complex **1** upon 642 nm red laser irradiation for 15 min duration. Lanes are: (1) DNA control (in light), (2) DNA + complex **1** (in light), (3) DNA + complex **1** (in dark) [I and II are the SC and NC forms of pUC19 DNA respectively]. Panels (b) and (c): Gel diagram showing mechanistic aspects of the photocleavage of pUC19 DNA in presence of complex **1** and different scavengers/quenchers/additives, namely, KI, 4 mM; TEMP, 4 mM; NaN_3, 4 mM; DHN, 4 mM; D_2O, 4 μL; DMSO, 4 μL; SOD, 4 units; catalase, 4 units; Tiron, 4 mM using red laser light (642 nm) irradiation. Lanes are: (4) DNA + complex **1** + NaN_3, (5) DNA + complex **1** + TEMP, (6) DNA + complex **1** + DHN (1,5-dihydroxynapthalene), (7) DNA + complex **1** + D_2O, (8) DNA + complex **1** + KI, (9) DNA + complex **1** + DMSO, (10) DNA + complex **1** + catalase, (11) DNA + complex **1** + Tiron, and (12) DNA + complex **1** + SOD.

Figure S36. Cell viability plots obtained from the MTT assay of ligand **HL[1]** in HeLa cells upon light (L, 600-720 nm, 20 min exposure, light dose: 30 J cm^{-2}) exposure and in dark (D) condition.

Figure S37. Cell viability plots obtained from MTT assay of ligand **HL[1]** in MCF-7 cell line upon light exposure (L, 600-720 nm, 20 min exposure, light dose: 30 J cm^{-2}) and in dark (D) condition.

Figure S38. Cell viability plots obtained from MTT assay of complex **1** in HeLa cells under light (L, 600-720 nm, 20 min exposure, light dose: 30 J cm^{-2}) and in dark (D) condition.

Figure S39. Cell viability plots obtained from MTT assay of complex **1** in MCF-7 cell line under light (L, 600-720 nm, 20 min exposure, light dose: 30 J cm^{-2}) and in dark (D) condition.

Figure S40. Cell viability plots obtained from MTT assay of **HL[1]** in HPL1D cell line under light (L, 600-720 nm, 20 min exposure, light dose: 30 J cm^{-2}) and in dark (D) condition.

Figure S41. Cell viability plots obtained from MTT assay of complex **1** in HPL1D cell line under light (L, 600-720 nm, 20 min exposure, light dose: 30 J cm^{-2}) and in dark (D) condition.

Figure S42. Time-dependent cellular uptake study of complex **1** in HeLa cells by FACS analysis.

Figure S43. CLSM series images obtained from live cellular uptake of complex **1** (2 μM) in HeLa cells with no time interval with band path of 660 nm to 750 nm by using λ_{ex} of 633 nm. Scale bar: 20 μm.

Figure S44. Merged images with emissive trackers along with 2D scattered plot for Pearson's correlation coefficient (PCC) calculations for complex **1**.

Figure S45. Confocal images for HeLa cells with suitable trackers and complex **1**. Panel (i) shows red emission of complex **1**, panel (ii) shows blue emission of nucleus staining dye Hoechst, panel (iii) shows green emission of Lysosome tracker, panel (iv) shows merged image, and panel (v) shows bright field.

Figure S46. Effect of the metal complex on caspase-3/7 activity in HeLa cells upon treatment with $0.5\times IC_{50}$ concentration.

Figure S47. Annexin V-FITC/propidium iodide assay in HeLa cells: (a) cells only; (b) cells + annexin V-FITC; (c) cells + propidium iodide; (d) cells + annexin V-FITC + propidium iodide. The % cell population is shown in respective quadrants [lower left: live cells, lower right: early apoptotic cells, upper right: late apoptotic cells, upper left, dead cells].

Figure S48. Cell cycle progression in HeLa cells in control set.

Table S1. Selected physicochemical data for complex **1** and ligand $\mathbf{HL^1}$

Table S2. Selected bonding parameters namely, bond lengths (Å) and bond angles (°) for ligand precursor $\mathbf{Me\text{-}L^1}$

Table S3. Coordinates of optimized Geometry for complex **1** obtained from DFT calculation using B3LYP/LanL2DZ level of theory for all atoms

Table S4. Excitation energies and oscillator strengths obtained from TD-DFT calculations for complex **1**

Singlet oxygen quantum yield determination. Singlet oxygen quantum yield was determined from 1,3-diphenylisobenzofuran (DPBF) titration experiment. It acted as a singlet oxygen scavenger which reacts with singlet oxygen to form 1,2-dibenzoylbenzene. Complex $[Pt(NH_3)_2Cl_2(OH)(\mathbf{L^1})]$ (**1)** and ligand $\mathbf{HL^1}$ were dissolved in 50:1 molar concentration ratio in DMSO and shined with 642 nm laser source. Photooxidation of DPBF was monitored by decrease in absorbance maxima at 417 nm at 3 seconds time intervals. For quantum yield determination, methylene blue ($\Phi_\Delta = 0.52$) was used as a standard. A decrease in the DPBF absorption maxima intensity around 417 nm was plotted against the irradiation time. The singlet oxygen quantum yield values (Φ_Δ) were obtained by using following equation,

$$\Phi_{\Delta c} = \Phi_{\Delta MB} \times (m_c/m_{MB}) \times (F_{MB}/F_c) \ldots (1)$$

Here, subscript "c" refers to complex **1** and ligand $\mathbf{HL^1}$ and subscript "MB" refers to methylene blue, Φ_Δ is the value of singlet oxygen quantum yield, m is the slope of ΔOD vs. time plot and

"F" is the absorption correction factor. It can be expressed as $F = 1\text{-}10^{-OD}$, where OD is the optical density (absorbance) at irradiation wavelength.

X-ray crystallographic procedure and theoretical calculations

Single crystals of **Me-L^1** were obtained from saturated acetone solution of the compound. A suitable crystal of the compound was mounted on a loop dipped in paratone oil. Data collection was performed in Bruker SMART APEX CCD diffractometer having a 1.75 kW sealed tube. Mo-Kα was used as X-ray source (0.71073 Å wavelength) with increasing ω and width of 0.3° per frame. Intensity data collection was performed in ω-2θ scan mode. Lorentz polarization and absorption correction was performed.[S1] For solving the structure and refinement, WinGx suite of programs (version 1.63.04a) and SHELXL-2014/7 were used.[S2,S3] Anisotropic displacement coefficients were used for the refinement of non-hydrogen atoms. Coordinates of non-hydrogen atoms were allowed to ride on their respective carbon atoms. Final refinement was done by considering anisotropic thermal parameters for all the non-hydrogen atoms, atomic positions for all the atoms and isotropic thermal parameters of all the hydrogen atoms present in the structure. For perspective view of the structure, ORTEP was used.[S2] Density functional theory (DFT) calculation was performed using Gaussian09 suite with B3LYP (Becke,3-parameter, Lee-Yang-Parr hybrid functional) level of theory and LanL2DZ basis set. Time-dependent density functional theory was performed at B3LYP/LanL2DZ level using IEF-PCM (integral equation formalism-polarizable continuum model) by incorporating the bulk solvent effect of DMSO in calculation.[S4]

DNA photocleavage experiment

Gel electrophoresis method was used to study the photo-induced DNA cleavage and chemical nuclease action of complex **1** on supercoiled plasmid DNA (pUC19) in DMF/Tris-HCl buffer medium at pH = 7.2. Photo-illumination was carried out in red

light of 642 nm diode laser (100 mW) source having beam diameter of 0.32±0.02 nm. For the experiment, each sample contained 30 μM of SC DNA, 50 mM NaCl in DMF-tris-HCl buffer, and complex **1** (25 μM). The volume was maintained at 20 μL. Samples were kept for 1 h incubation at 37 °C before light exposure. After 15 min light irradiation and 1 h post-incubation, 2 μL loading dye (bromophenol blue (25%), glycerol (30 %), xylene cyanol (0.25%)) was added to each sample. Mechanistic investigations to identify the nature of ROS produced were done using different quenchers/scavengers, namely, DMSO (4 μL), KI (4 mM), TEMP (4 mM), DHN (dihydroxynaphthalene, 4 mM), NaN_3(4 mM), tiron (4 mM), SOD (4 units), catalase (4 units), that were added to pUC19 DNA before the addition of complex **1** in the respective experiment. Another set of experiment was performed by adding 4 μL D_2O in which singlet oxygen has longer lifetime.

Measurement of partition coefficient

Partition coefficient for the complex was measured by shake-flask method. Water saturated octanol was prepared by mixing 4 ml octanol and 1 ml of water for 24 h. Octanol saturated water was prepared in a similar manner. The complex was solubilized in 2 ml of saturated octanol by addition of minimal volume of DMSO and added to 2 ml saturated water. The mixture was shaken for 24 h by a mechanical shaker and allowed to settle and they were separated. Complex concentration was determined by UV-vis absorption spectroscopy. Partition co-efficient was calculated by the following equation,

$$\log P_{o/w} = \log([\text{complex}]_{\text{octanol}}/[\text{complex}]_{\text{water}}) \quad \ldots (2)$$

Schemes and Figures

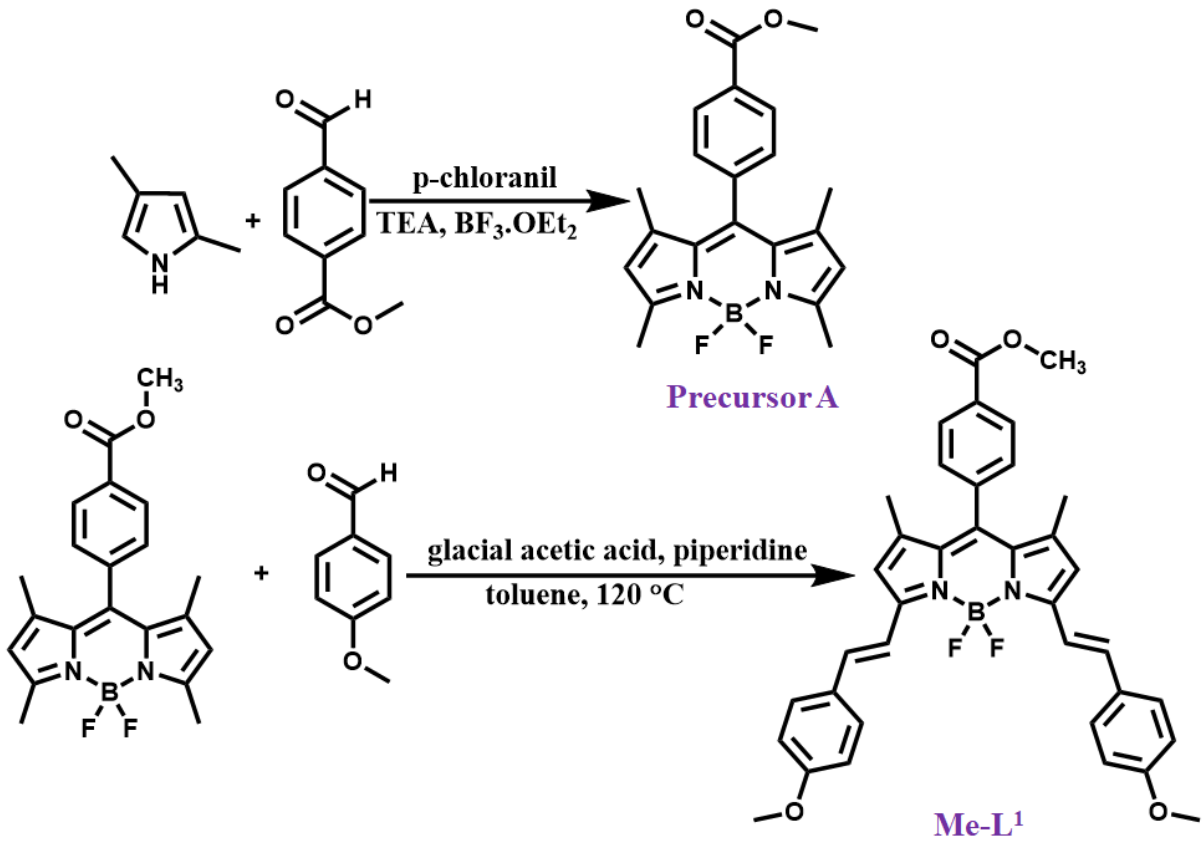

Scheme S1. Scheme for the synthesis of precursor A and **Me-L**[1].

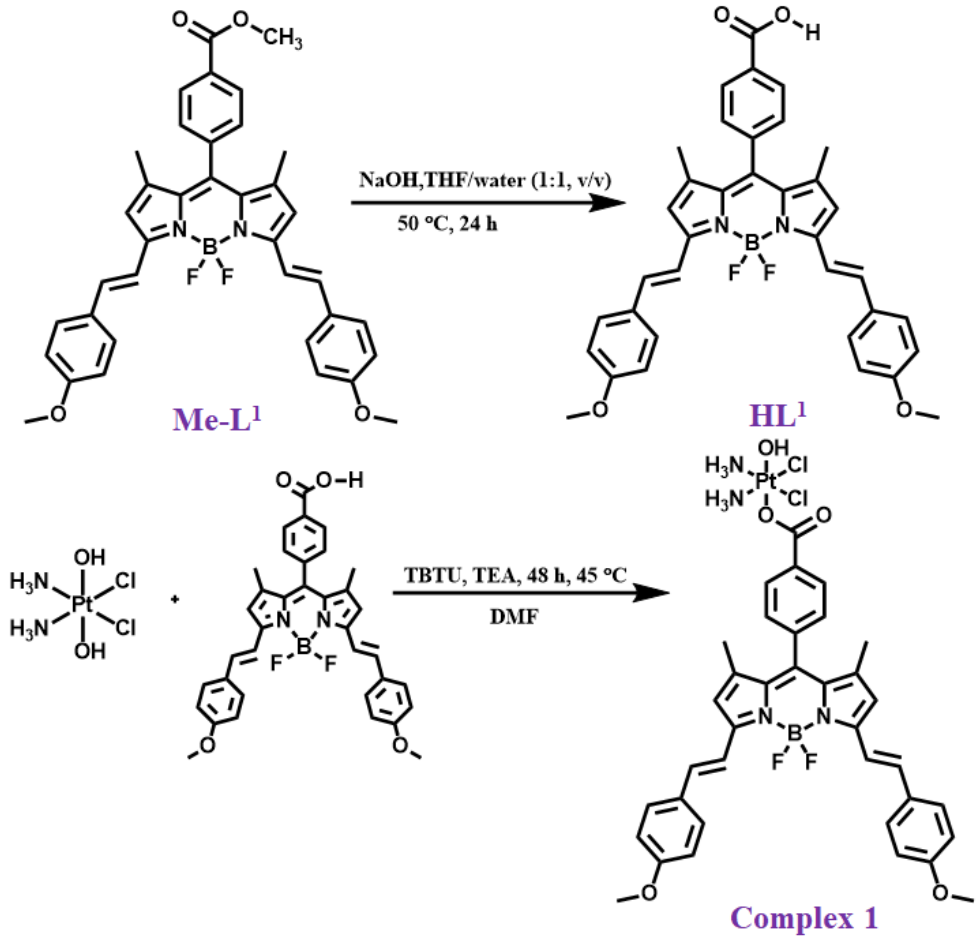

Scheme S2. Scheme for the synthesis of **HL**[1] and complex **1**.

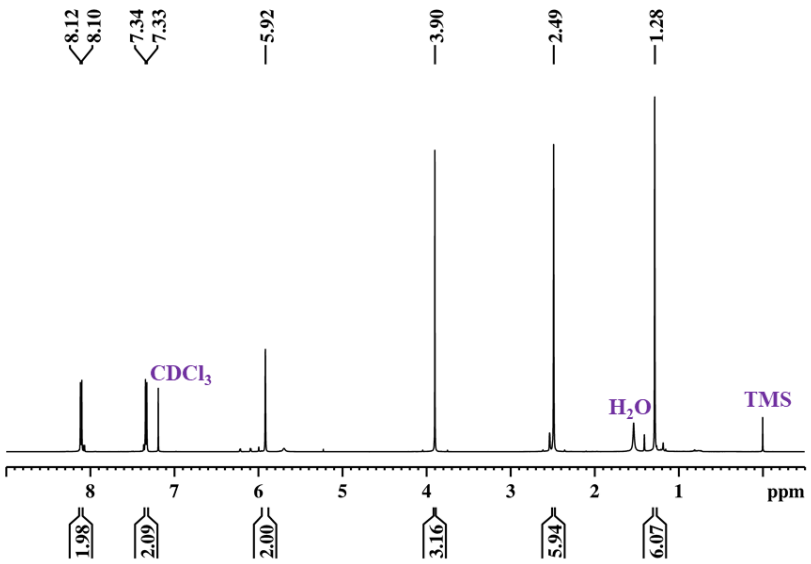

Figure S1. ^{1}H NMR spectrum of precursor **A** in $CDCl_3$.

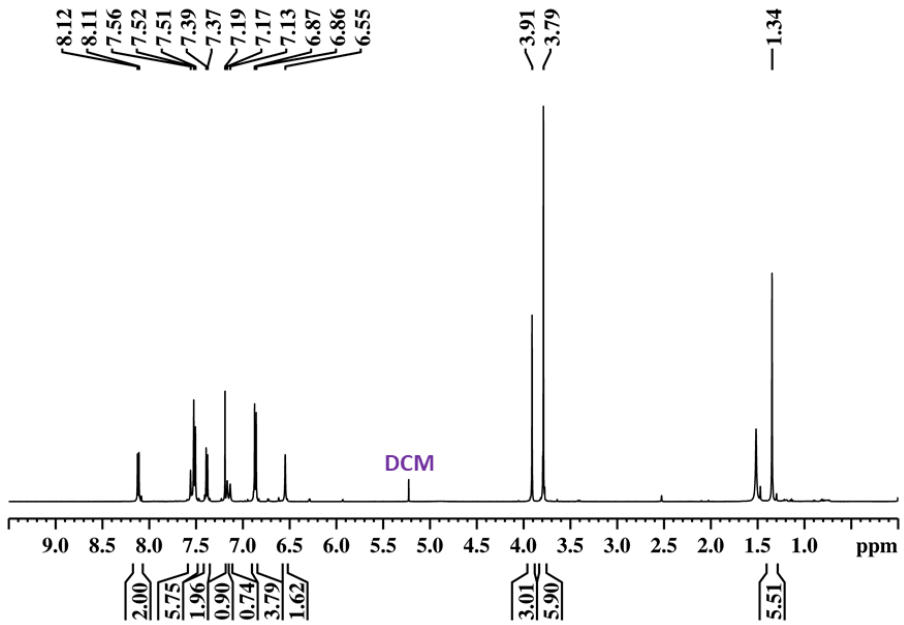

Figure S2. ^{1}H NMR spectrum of ligand precursor **Me-L^{1}** in $CDCl_3$ (DCM is dichloromethane).

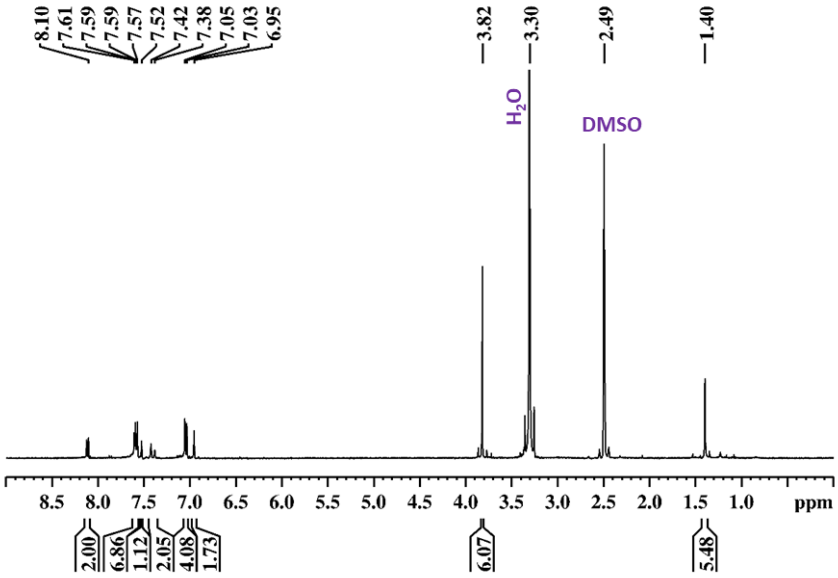

Figure S3. ^{1}H NMR spectrum of ligand **HL^{1}** in DMSO-d_6.

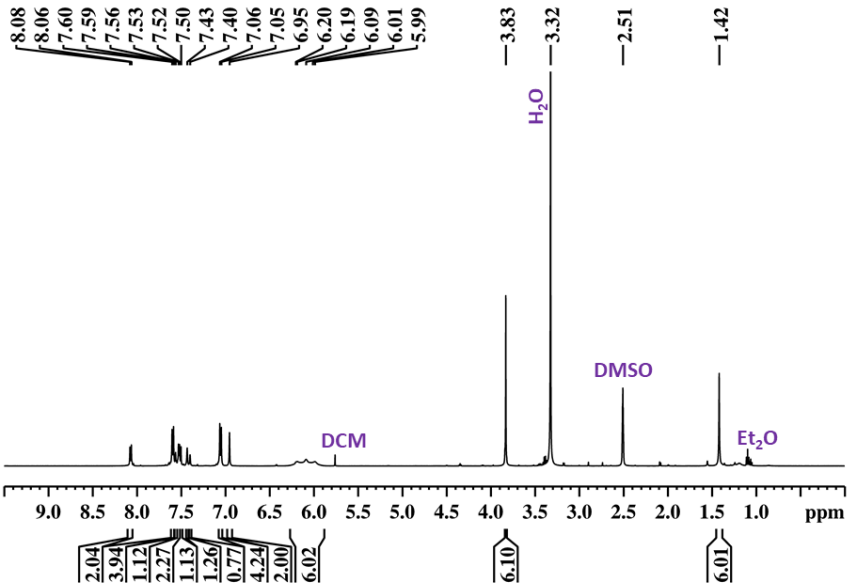

Figure S4. ^{1}H NMR spectrum of complex **1** in DMSO-d_6.

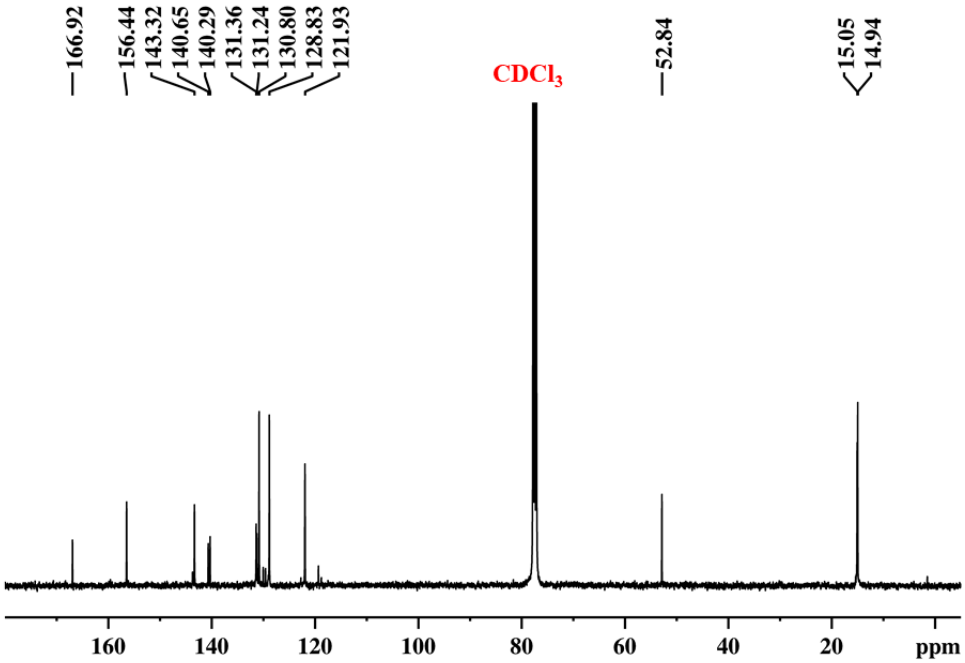

Figure S5. ^{13}C NMR spectrum of precursor **A** in $CDCl_3$.

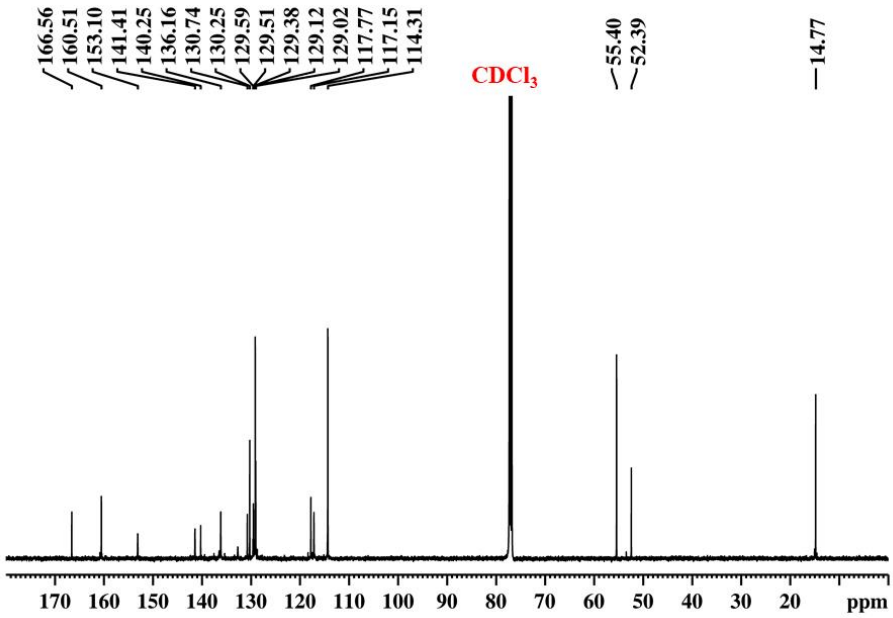

Figure S6. ^{13}C NMR spectrum of ligand precursor **Me-L^1** in $CDCl_3$.

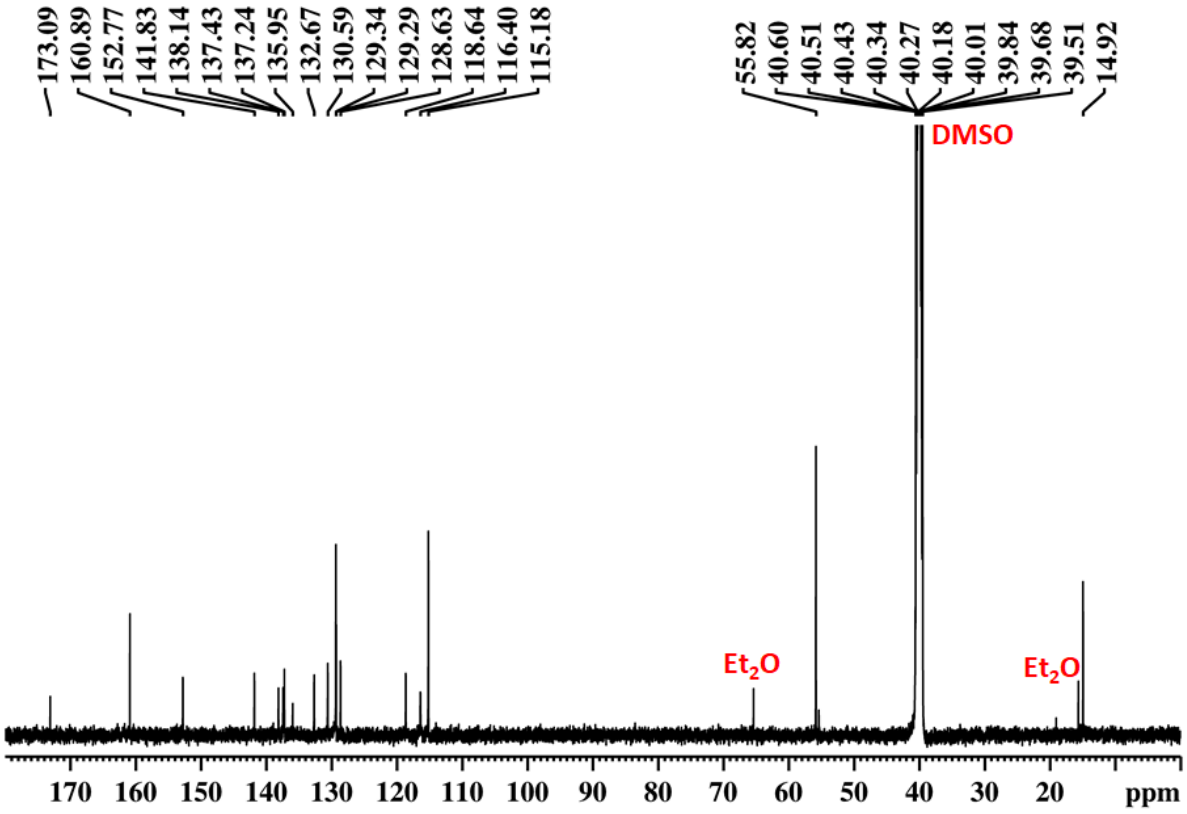

Figure S7. ^{13}C NMR spectrum of complex **1** in DMSO-d_6.

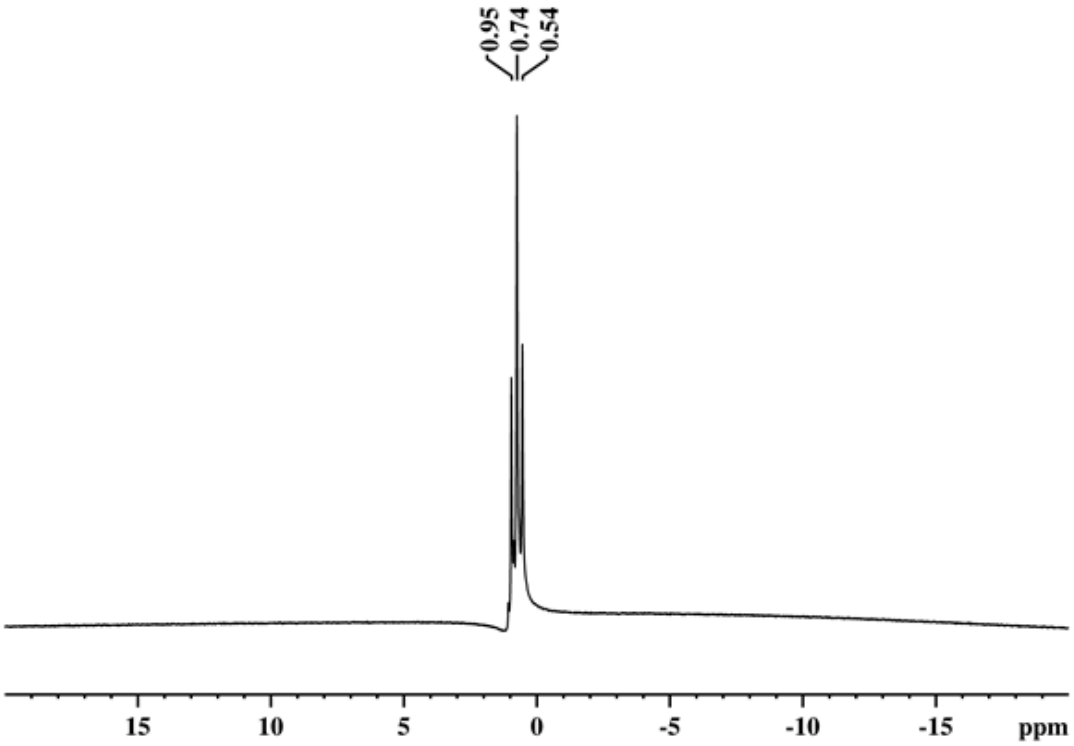

Figure S8. ^{11}B NMR spectrum of precursor **A** in $CDCl_3$.

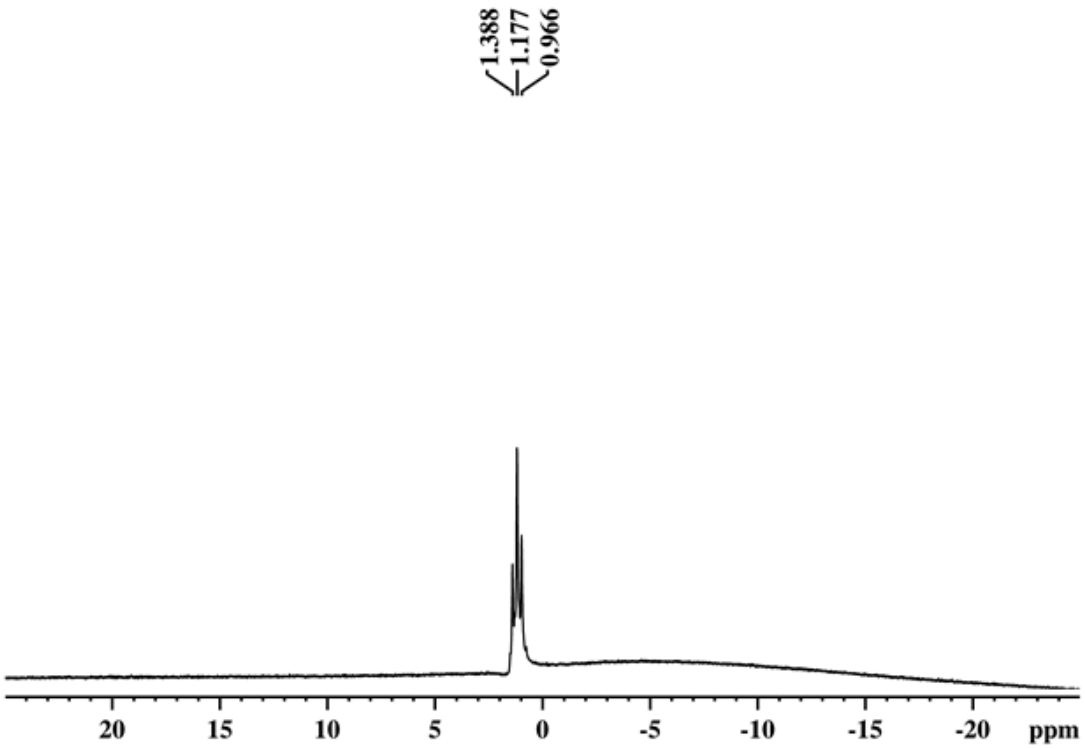

Figure S9. ^{11}B NMR spectrum of **Me-L^1** in $CDCl_3$.

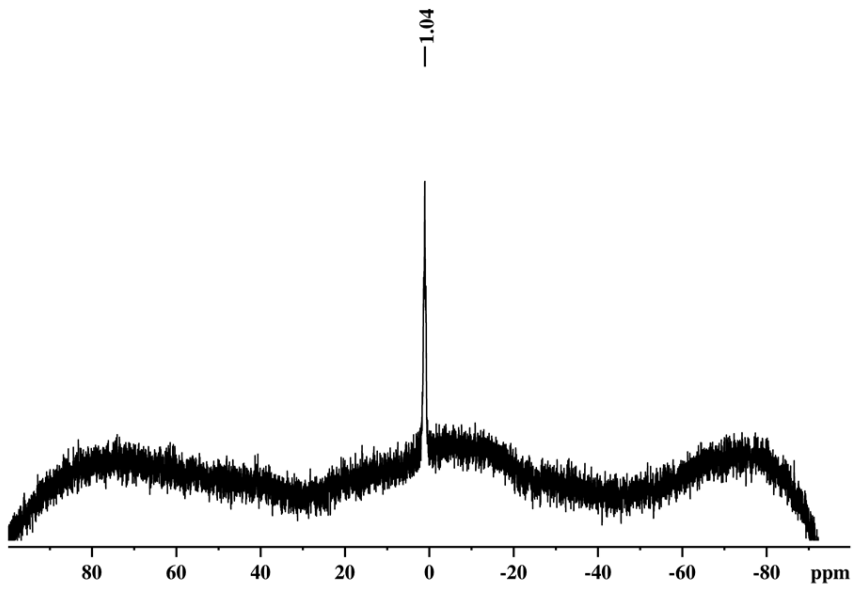

Figure S10. ^{11}B NMR spectrum of complex **1** in DMSO-d_6.

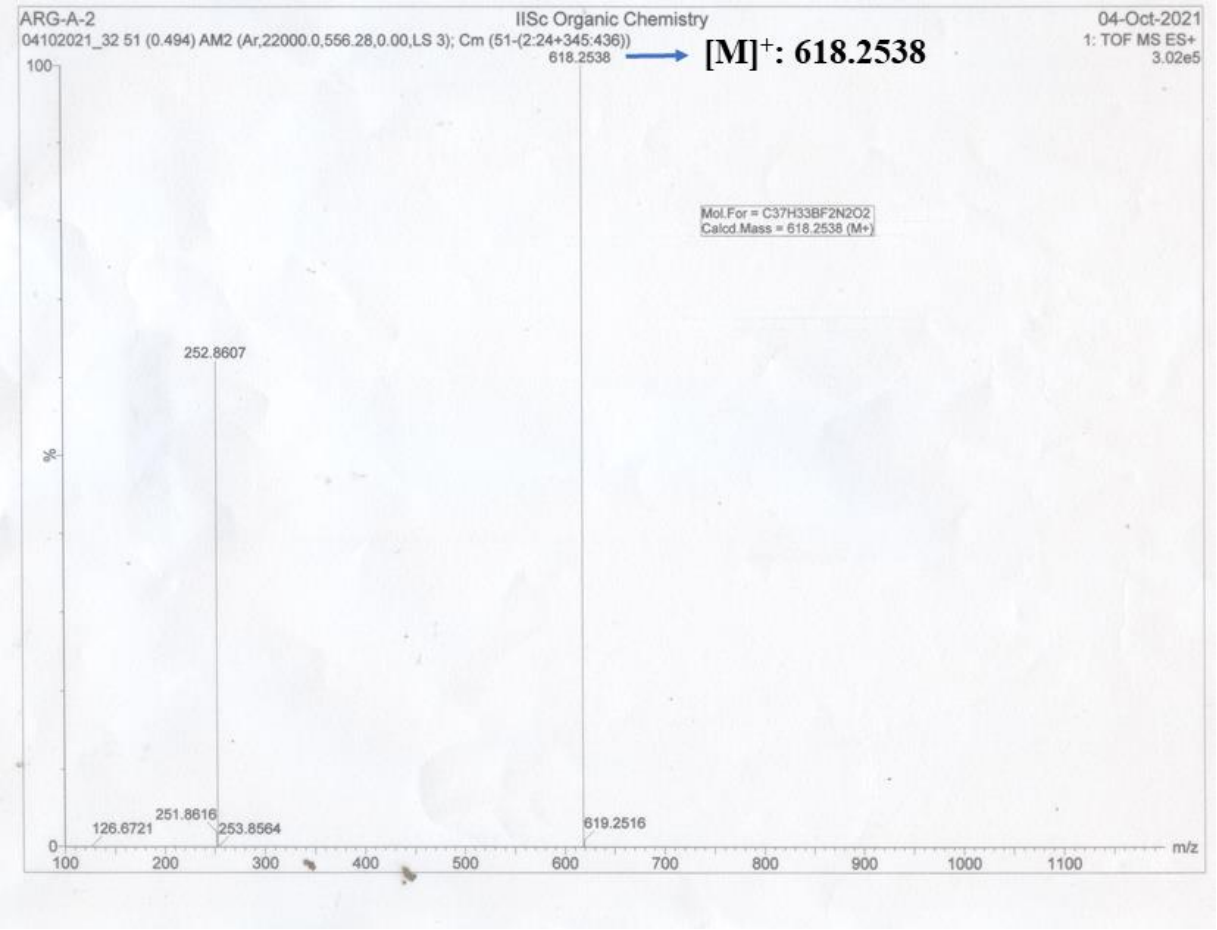

Figure S11. Mass spectrum of **Me-L[1]** recorded in acetonitrile with a peak corresponding to $[M]^+$ (m/z) at 618.2538.

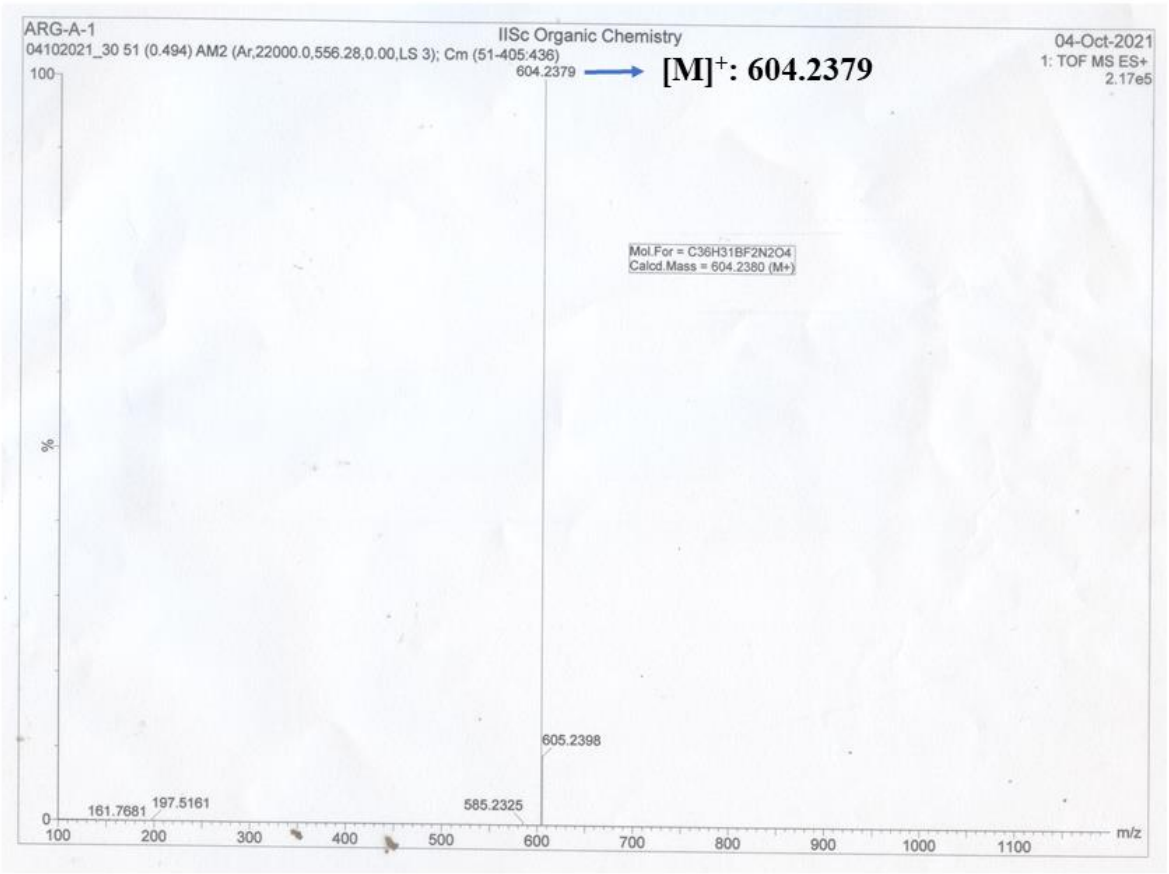

Figure S12. Mass spectrum of ligand **HL[1]** recorded in acetonitrile with a peak corresponding to $[M]^+$ (m/z) at 604.2379.

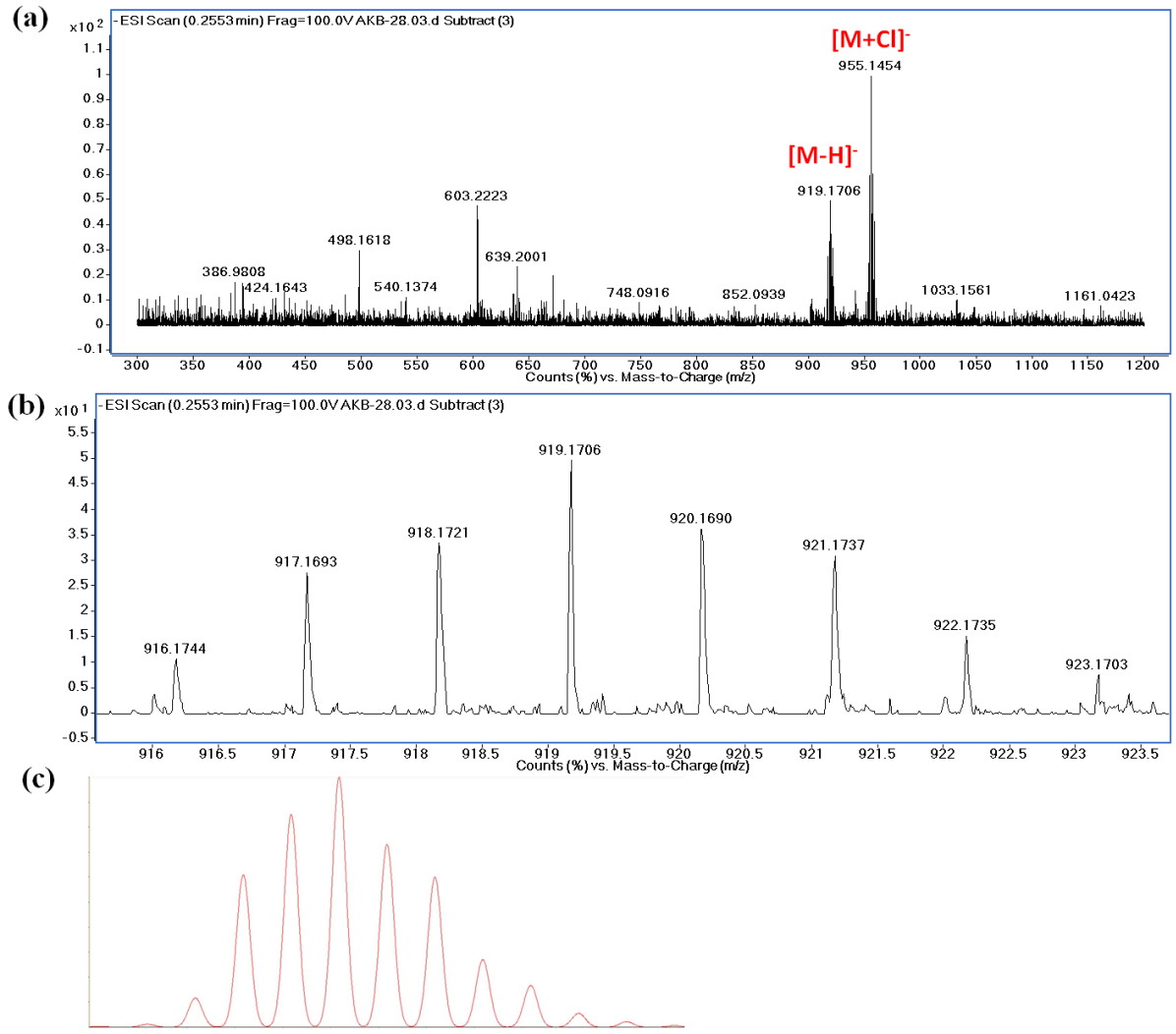

Figure S13. (a) Mass spectrum of complex **1** recorded in methanol with a peak corresponding to $[M-H]^-$ (m/z) at 919.1706. (b) Isotopic distribution of the complex indicating uninegative charge of the complex. (c) Simulated isotopic distribution pattern.

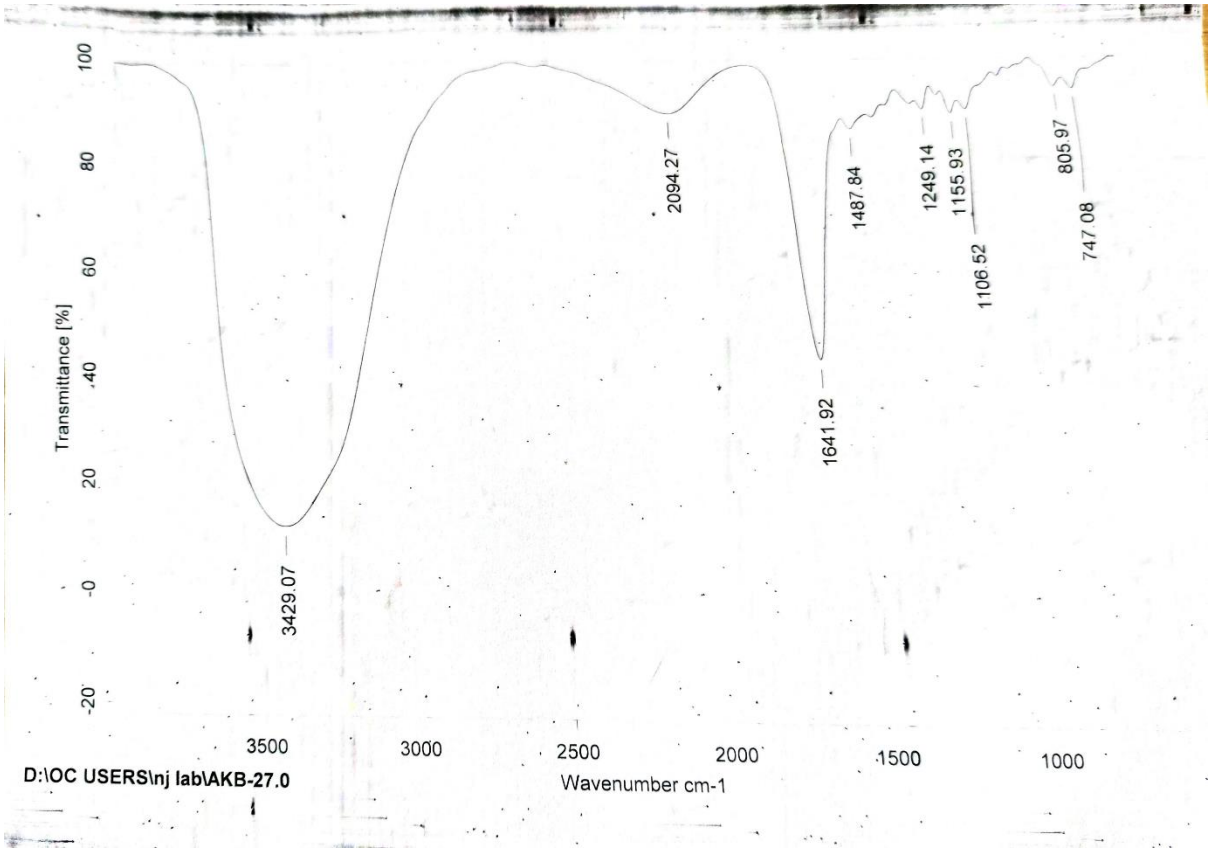

Figure S14. IR spectrum of the ligand **HL**[1] in KBr pellet.

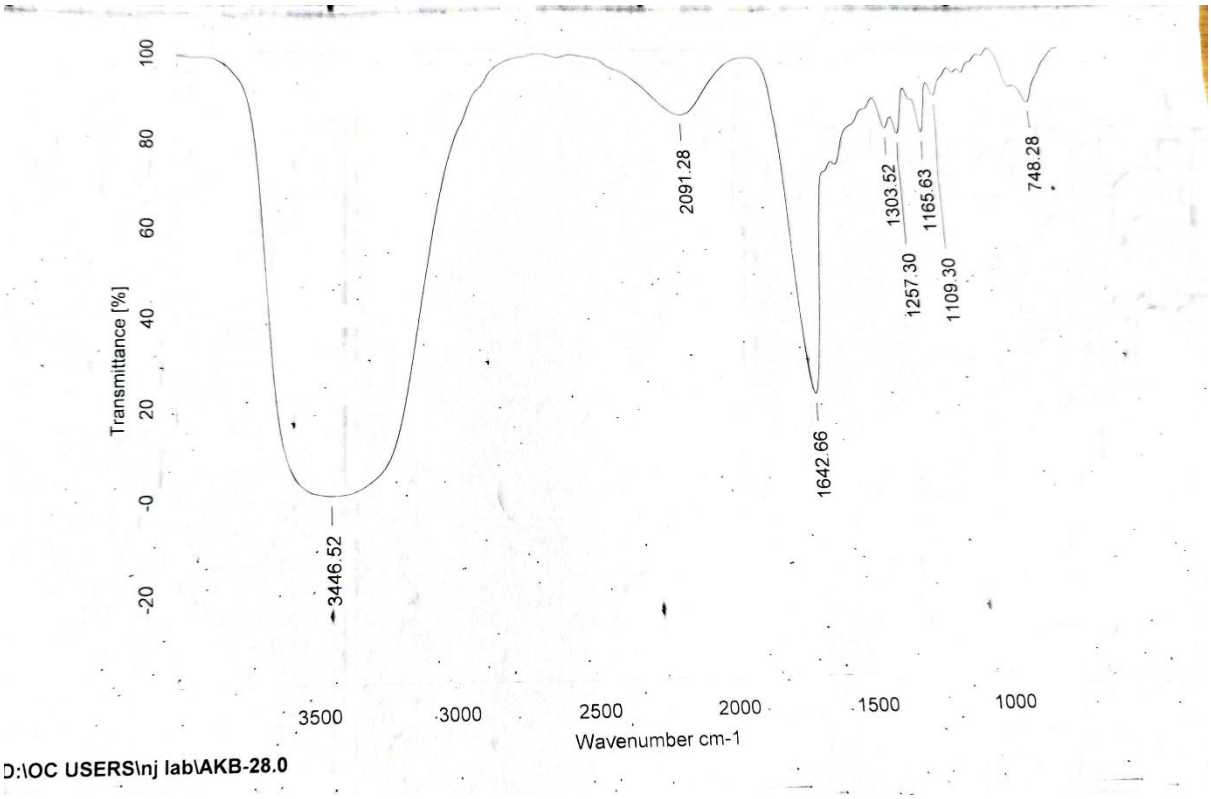

Figure S15. IR spectrum of the complex **1** in KBr pellet.

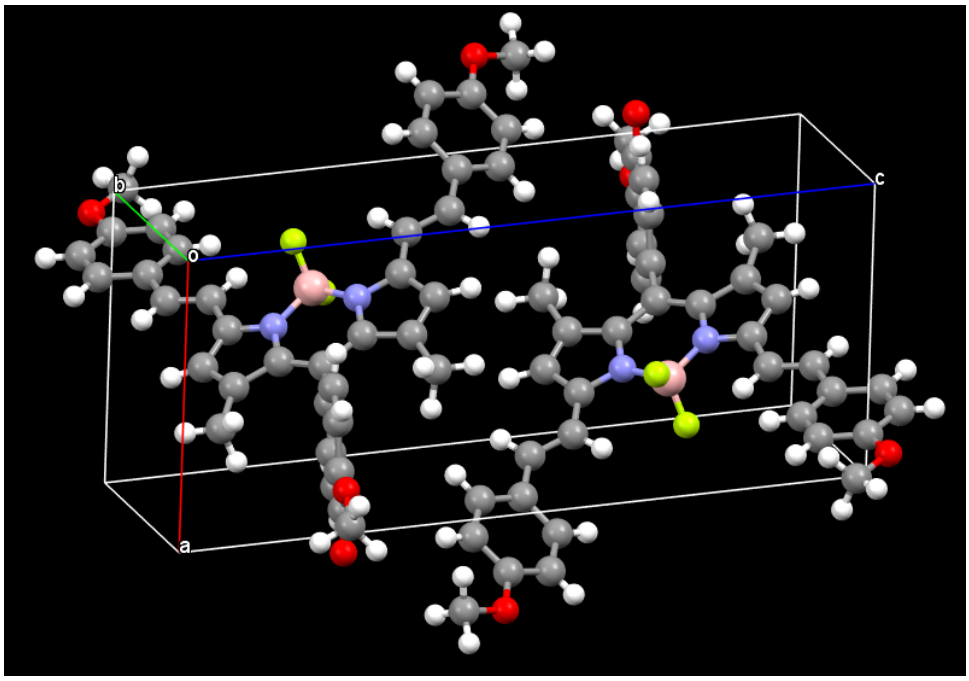

Figure S16. Unit cell packing diagram of **Me-L**[1]. Colour codes: C, grey; H, white; O, red; B, pink; F, lemon yellow; N, sky blue.

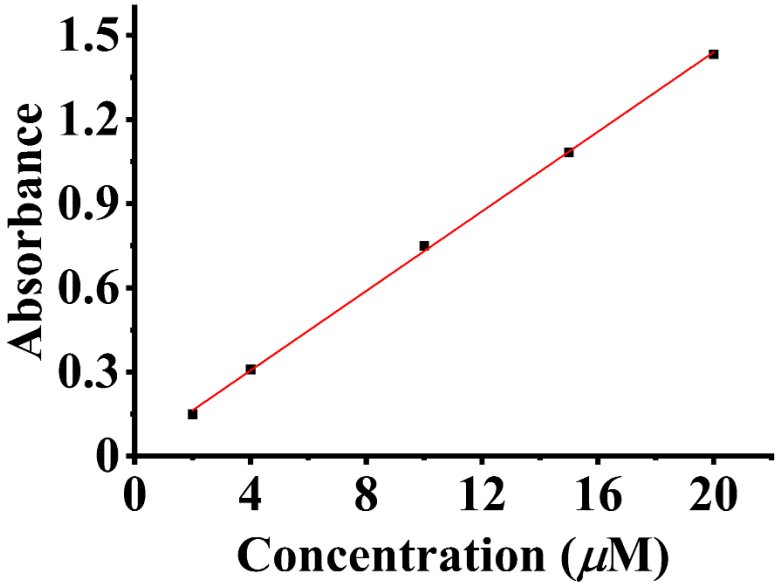

Figure S17. UV-vis spectra of complex **1** recorded at different concentration in DMSO, and absorbance was plotted against concentration.

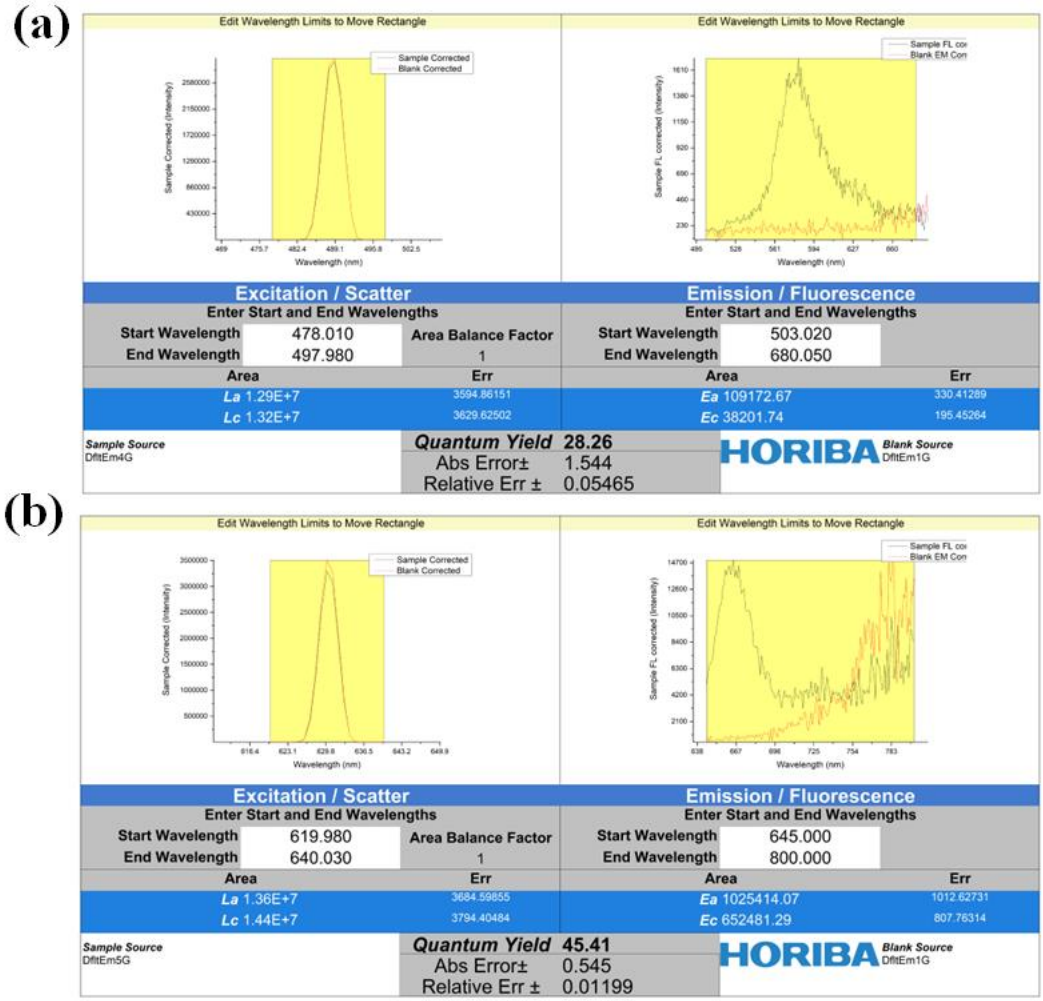

Figure S18. Fluorescence quantum yield for (a) rhodamine B in water and (b) ligand **HL**[1] in DMSO.

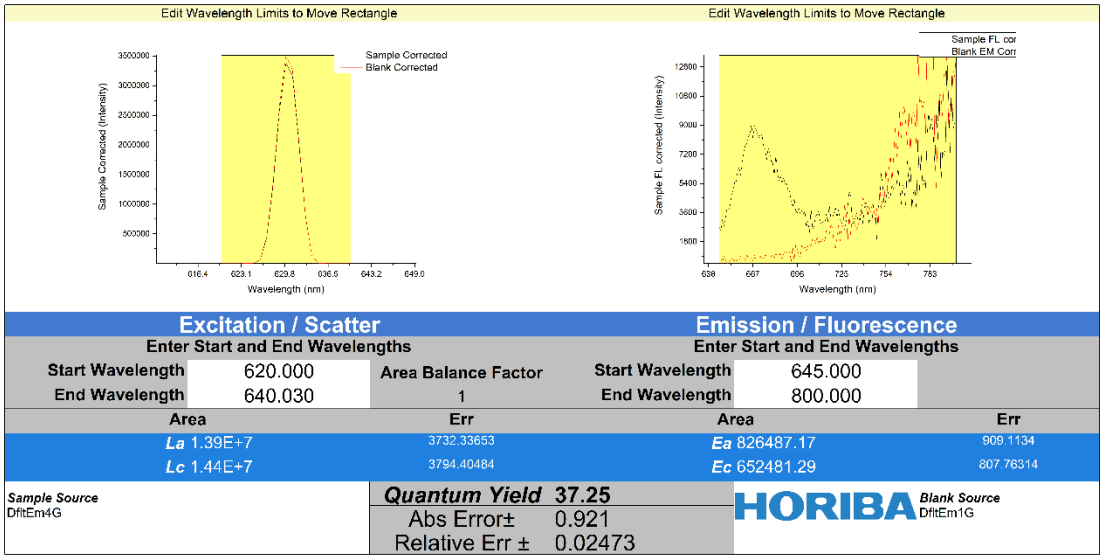

Figure S19. Fluorescence quantum yield of complex **1** in DMSO.

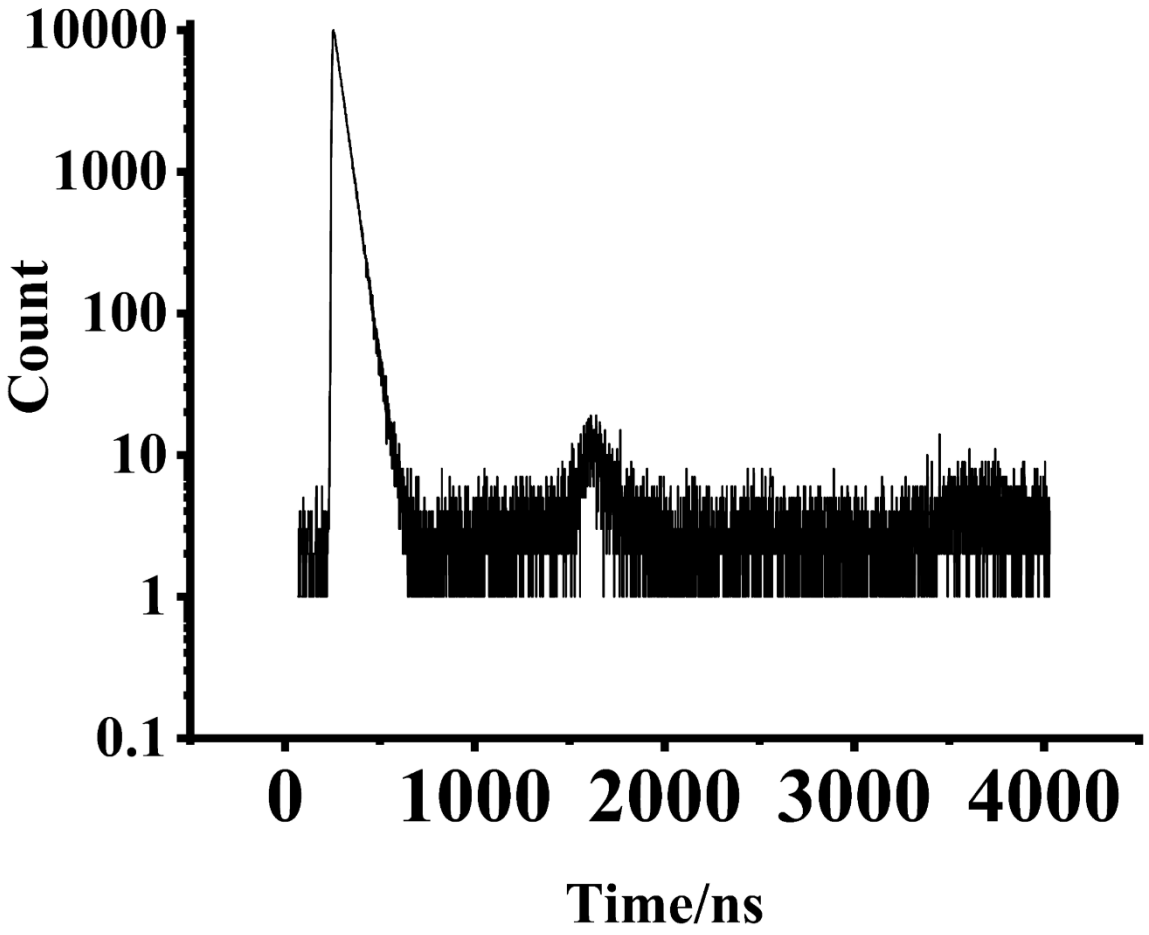

Figure S20. Excited state lifetime plot of complex **1** in DMF.

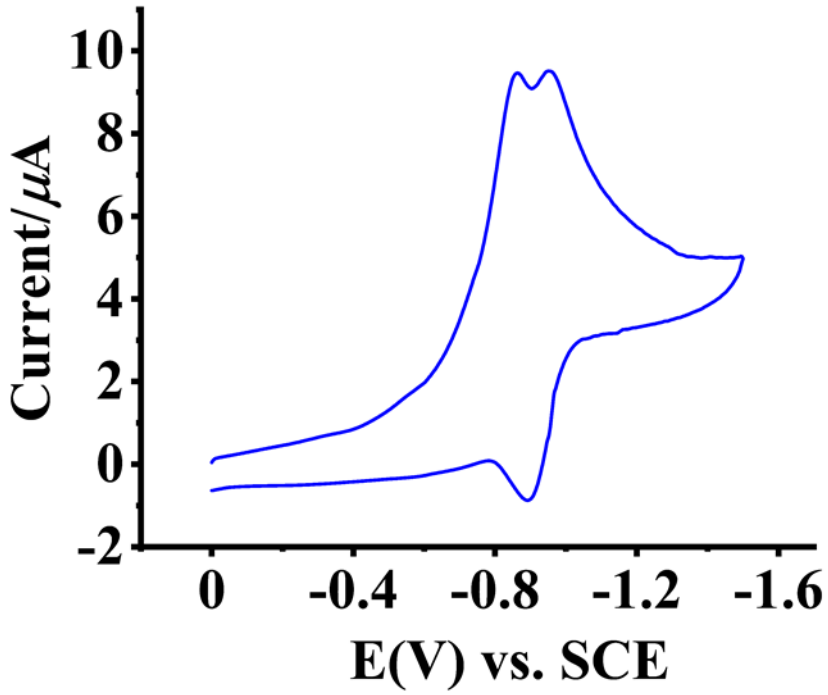

Figure S21. Cyclic voltammogram of complex **1** in DMF containing 0.15 M TBAHFP (tetrabutylammonium hexaflurophosphate) at a scan rate of 50 mV/sec using glassy carbon as the working electrode. The split peaks are assignable to the irreversible two-electron transfer for Pt(IV)→Pt(II) and reversible response from the BODIPY moiety. The reverse anodic peak corresponds to only BODIPY oxidation.

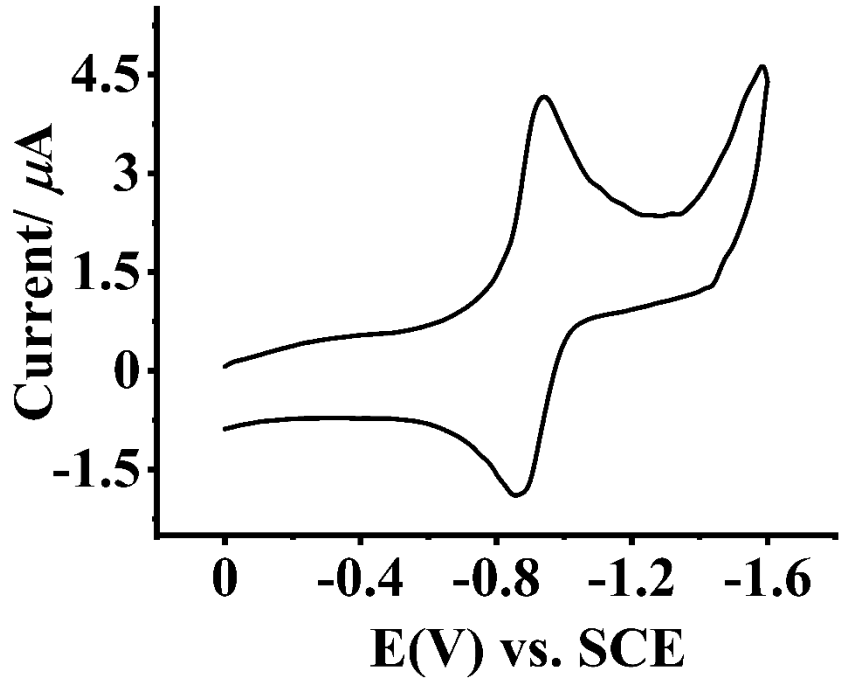

Figure S22. Cyclic voltammogram of ligand **HL**[1] in DMF containing 0.15 M TBAHFP at a scan rate of 50 mV/sec using glassy carbon as working electrode.

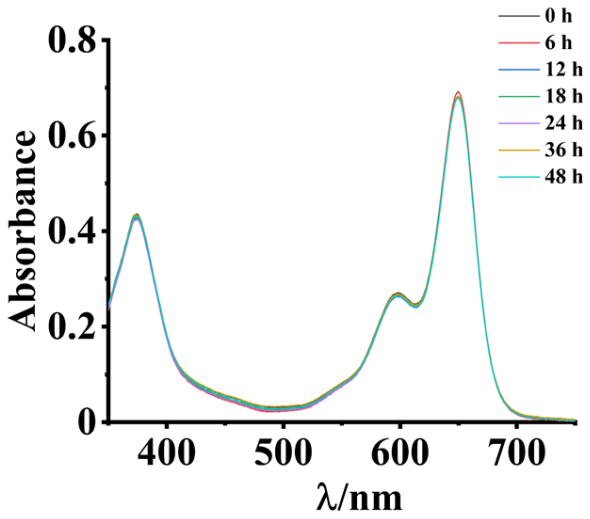

Figure S23. Time-dependent stability studies of complex **1** in 1:1 (v/v) DMSO/DPBS under dark condition.

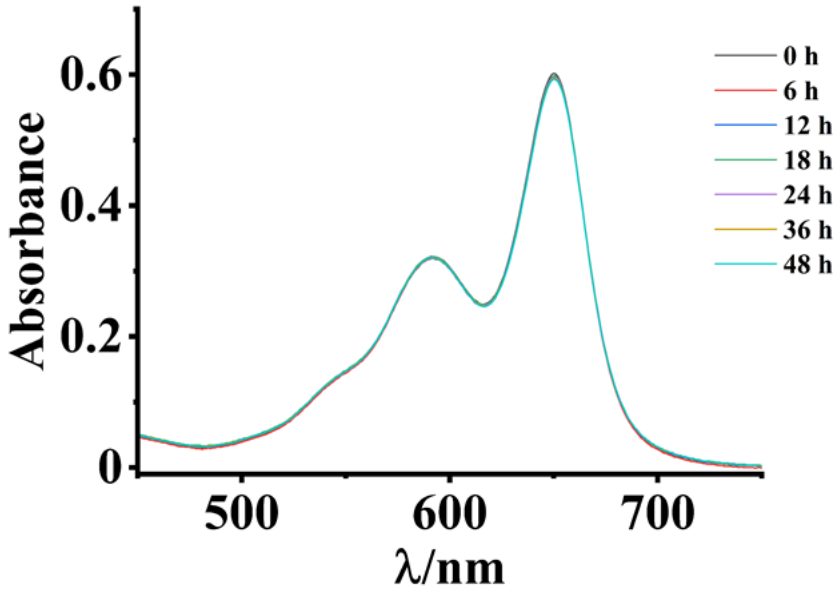

Figure S24. Time-dependent stability studies of complex **1** at pH = 3 in 1:1 (v/v) DMSO/DPBS under dark condition.

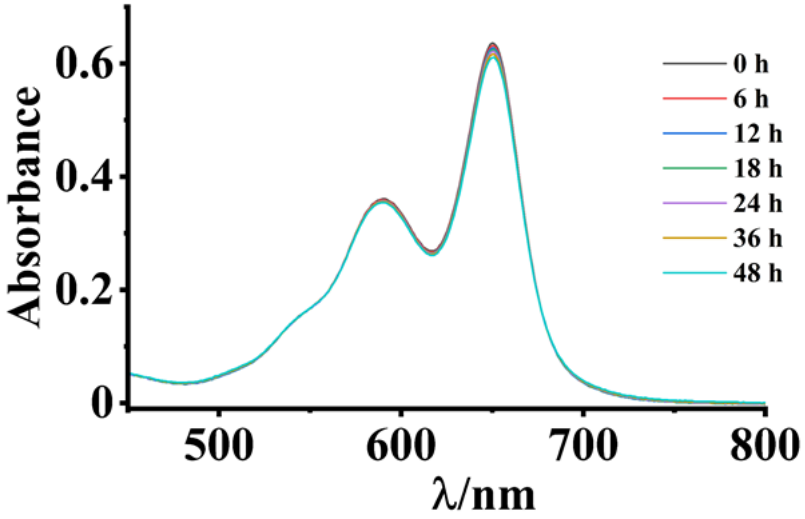

Figure S25. Time-dependent stability studies of complex **1** at pH = 9 in 1:1 (v/v) DMSO/DPBS under dark condition.

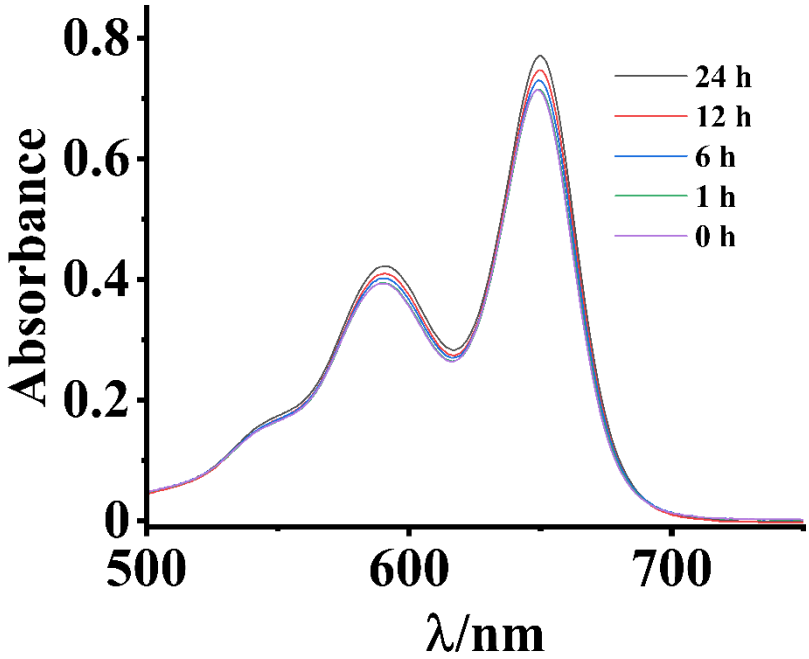

Figure S26. Time-dependent stability studies of complex **1** at 4 mM GSH concentration in 1:1 (v/v) DMSO/DPBS under dark condition.

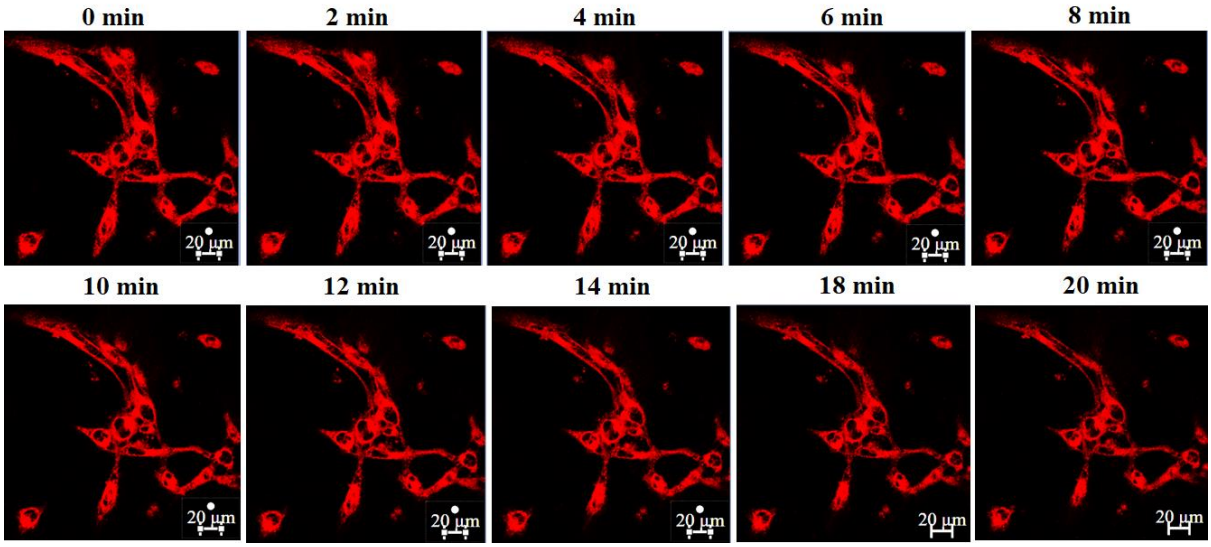

Figure S27. Confocal images of HeLa cells stained with IC_{50} concentration of complex **1** with increasing number of scans. A 633 nm laser with 6% output power was used for excitation, total experiment time ~20 min.

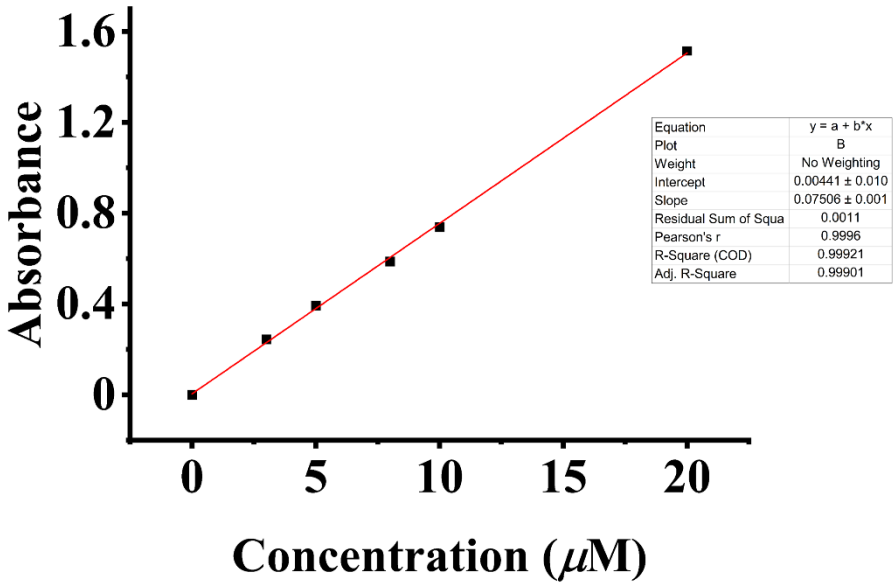

Figure S28. Calibration curve for complex **1** in octanol for lipophilicity measurement.

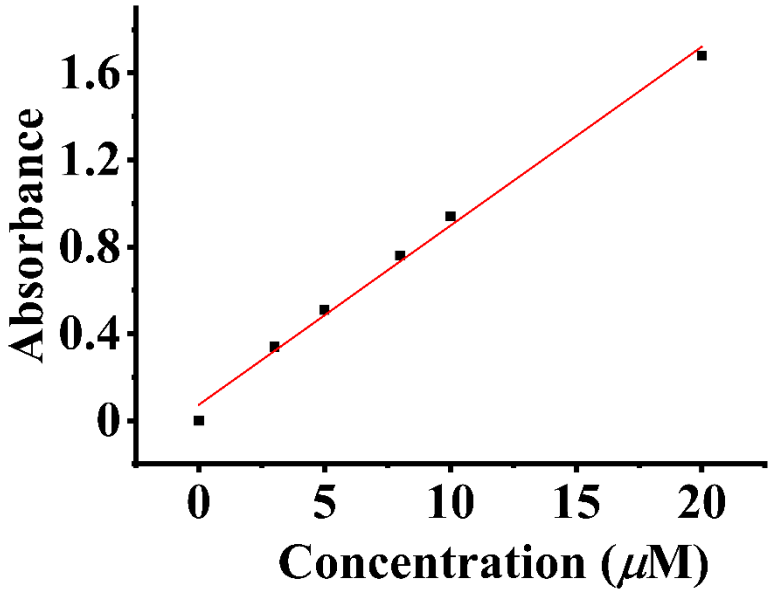

Figure S29. Calibration curve for ligand in octanol for lipophilicity measurement.

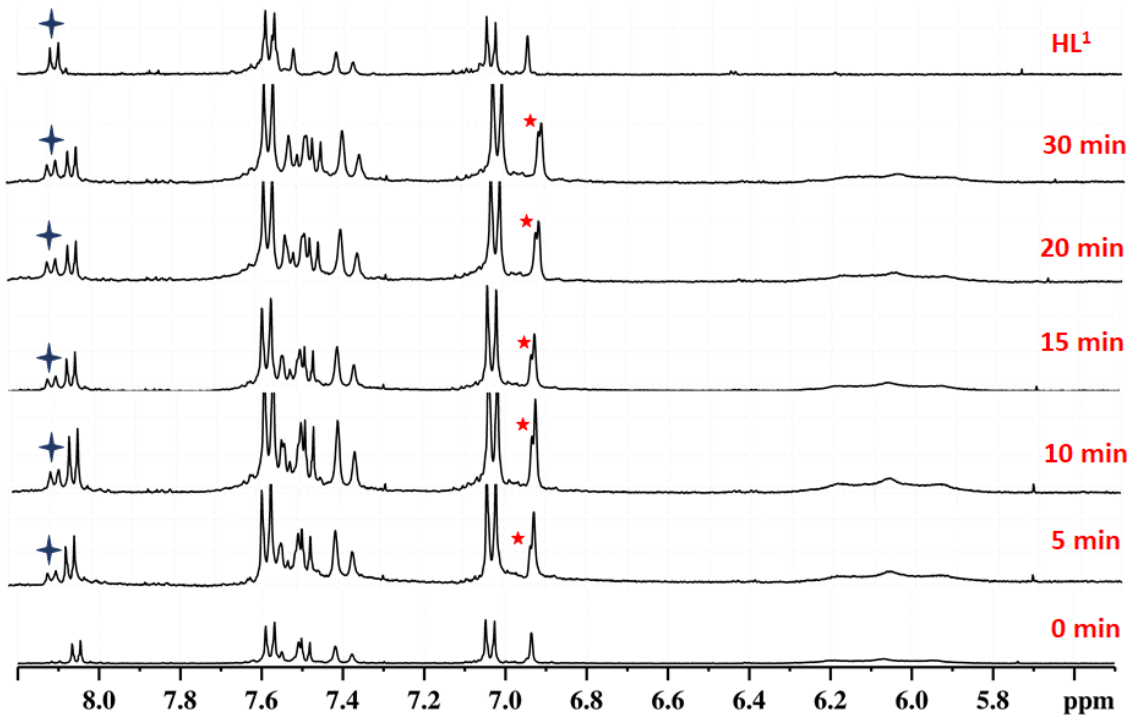

Figure S30. Time-dependent ^{1}H NMR spectra of complex **1** irradiated with 642 nm laser. Intensity of 8.11 ppm peak gradually increased and 6.94 ppm peak for γ-proton of **HL^{1}** gradually converted into a doublet.

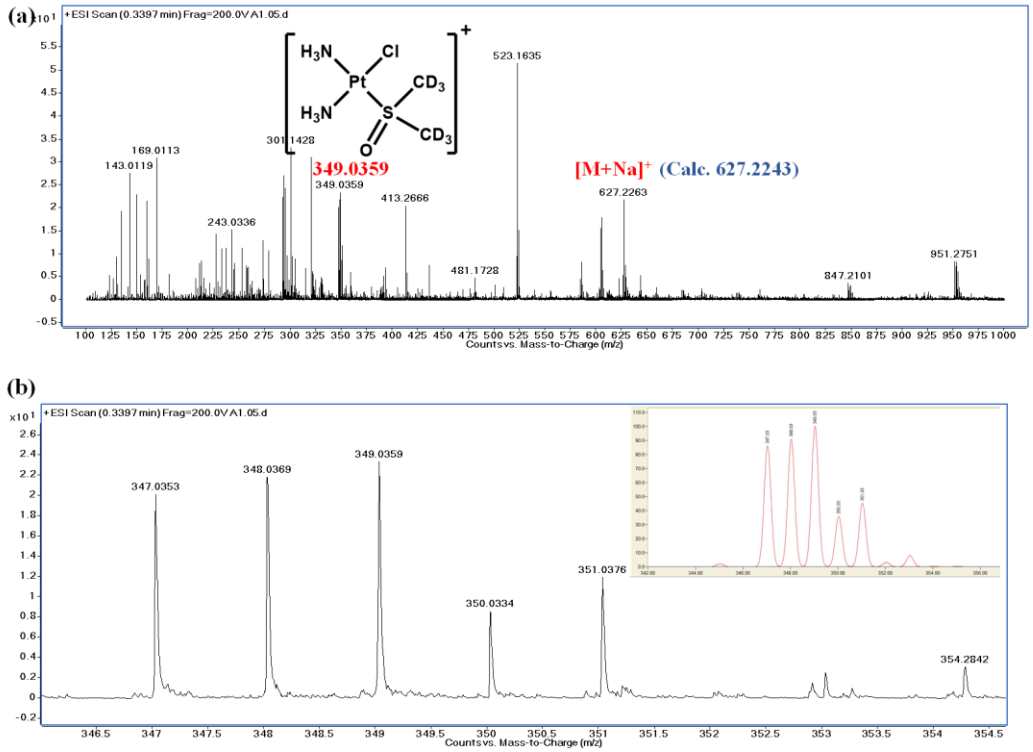

Figure S31. (a) ESI-MS spectrum of complex **1** solution (used for NMR study) after being irradiated with 642 nm laser source. The 349.0359 peak is assignable to $[Pt(NH_3)_2Cl(DMSO\text{-}d_6)]^+$ and 627.2263 peak is due to free ligand released from the complex after light irradiation. (b) Isotopic distribution of $[Pt(NH_3)_2Cl(DMSO\text{-}d_6)]^+$ adduct with the inset showing the simulated isotopic distribution.

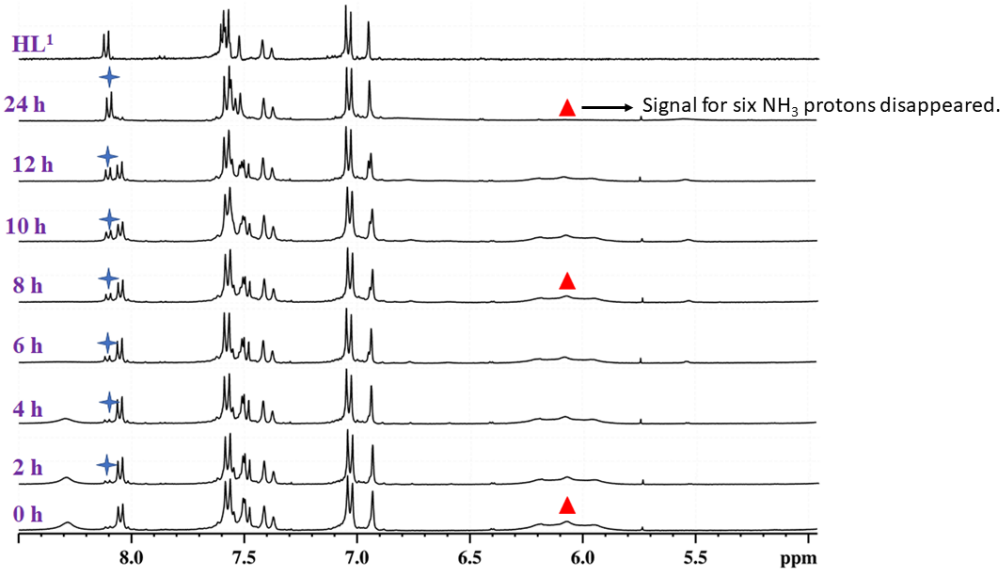

Figure S32. Time-dependent ^{1}H NMR spectra of the complex **1** in presence of 5 equiv. ascorbic acid. Signal for six ammine protons (marked with red) disappeared due to metal reduction in presence of ascorbic acid.

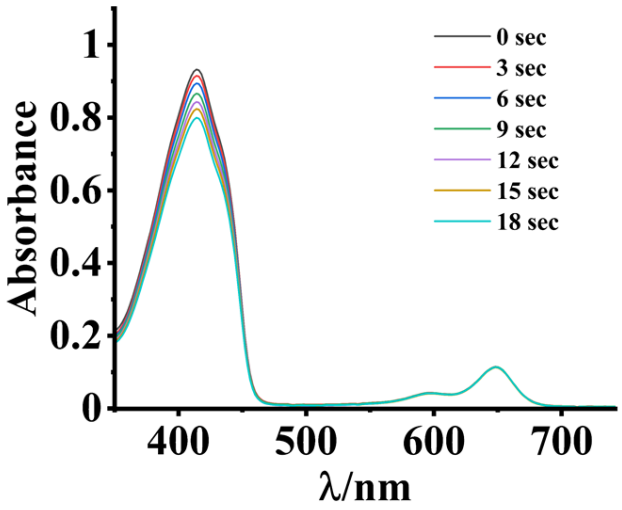

Figure S33. Changes in the absorption spectra of DBBF containing ligand **HL**[1] (50:1 concentration ratio) on red light exposure (642 nm, 100 mW) in DMSO.

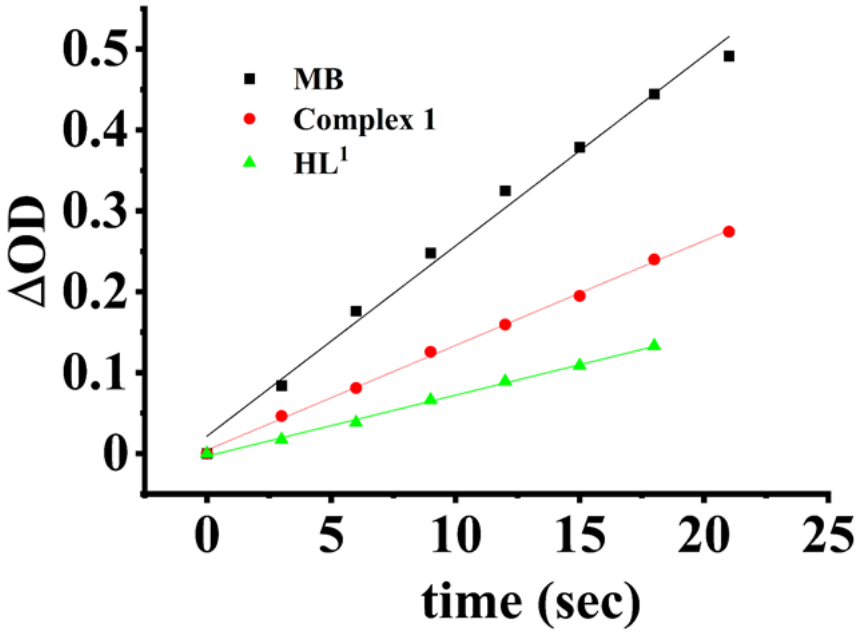

Figure S34. ΔOD vs. irradiation time for determining singlet oxygen quantum yield of complex **1** and **HL**[1] (MB, as control).

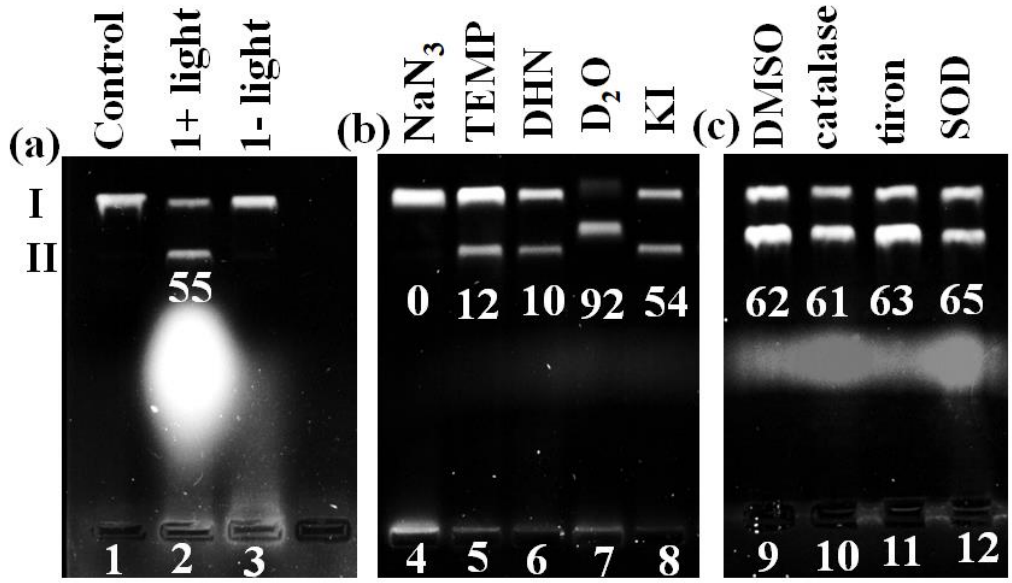

Figure S35. (a) Gel diagram showing photocleavage of pUC19 DNA in presence of complex **1** upon 642 nm red laser irradiation for 15 min duration. Lanes are: (1) DNA control (in light), (2) DNA + complex **1** (in light), (3) DNA + complex **1** (in dark) [I and II are the SC and NC forms of pUC19 DNA respectively]. Panels (b) and (c): Gel diagram showing mechanistic aspects of the photocleavage of pUC19 DNA in presence of complex **1** and different scavengers/quenchers/additives, namely, KI, 4 mM; TEMP, 4 mM; NaN_3, 4 mM; DHN, 4 mM; D_2O, 4 μL; DMSO, 4 μL; SOD, 4 units; catalase, 4 units; Tiron, 4 mM using red laser light (642 nm) irradiation. Lanes are: (4) DNA + complex **1** + NaN_3, (5) DNA + complex **1** + TEMP, (6) DNA + complex **1** + DHN (1,5-dihydroxynapthalene), (7) DNA + complex **1** + D_2O, (8) DNA + complex **1** + KI, (9) DNA + complex **1** + DMSO, (10) DNA + complex **1** + catalase, (11) DNA + complex **1** + Tiron, and (12) DNA + complex **1** + SOD.

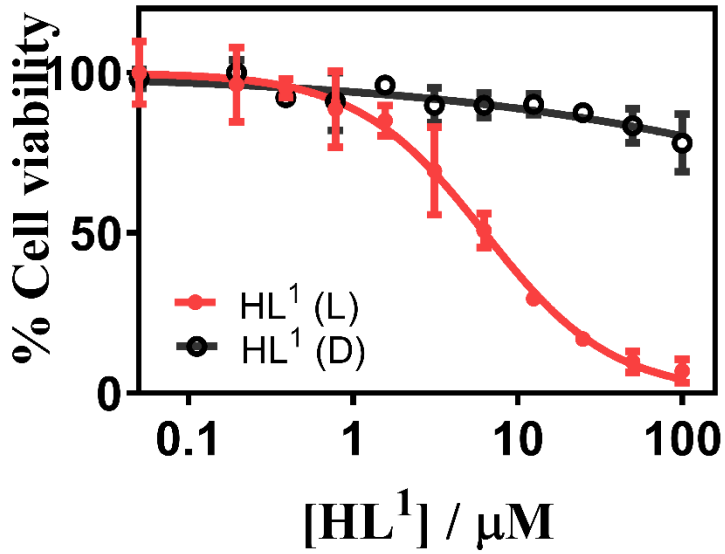

Figure S36. Cell viability plots obtained from MTT assay of ligand **HL**[1] in HeLa cells on light exposure (L, 600-720 nm, 20 min exposure, light dose: 30 J cm^{-2}) and in dark (D) condition.

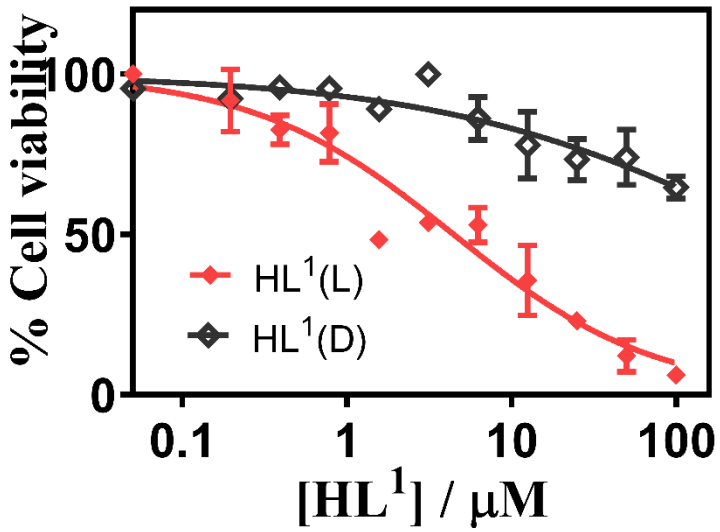

Figure S37. Cell viability plots obtained from MTT assay of ligand **HL**[1] in MCF-7 cell line on light irradiation (L, 600-720 nm, 20 min exposure, light dose: 30 J cm^{-2}) and in dark (D) condition.

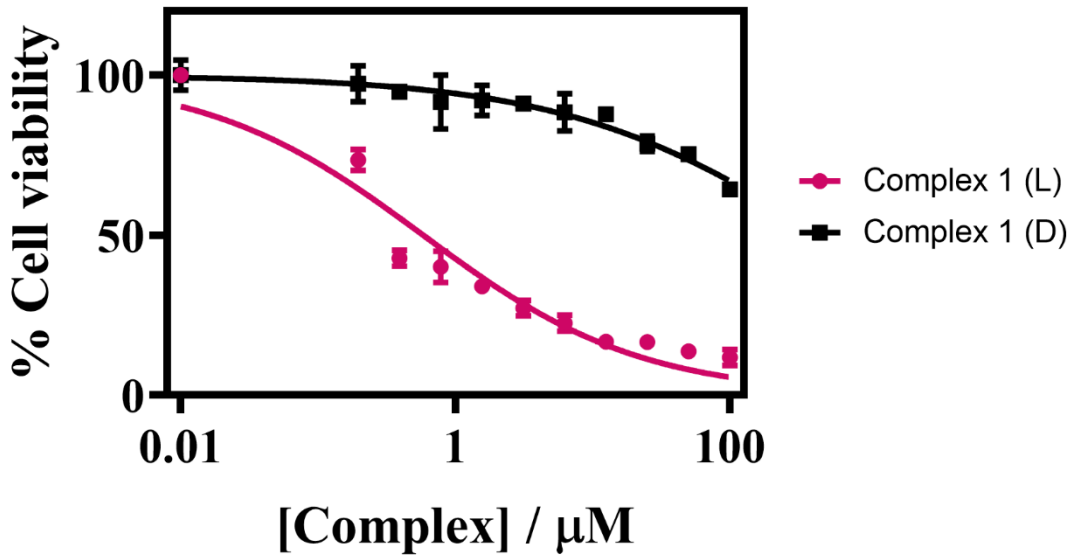

Figure S38. Cell viability plots obtained from MTT assay of complex **1** in HeLa cells on light irradiation (L, 600-720 nm, 20 min exposure, light dose: 30 J cm^{-2}) and in dark (D) condition.

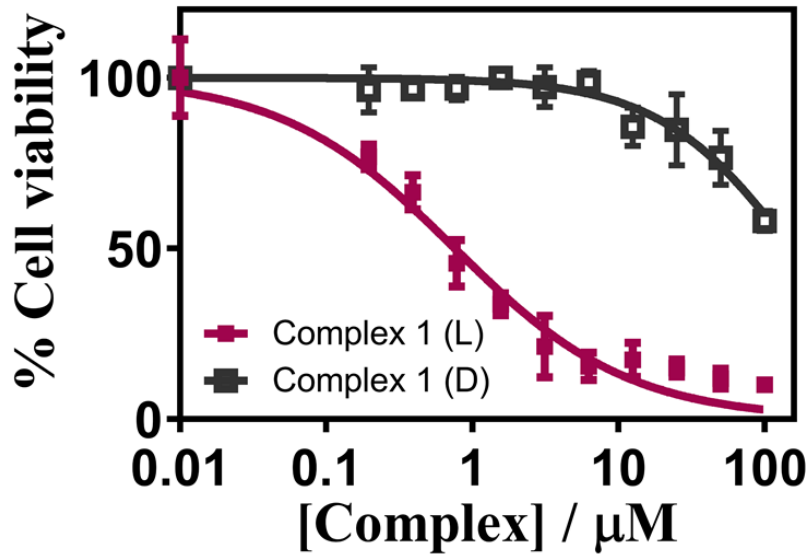

Figure S39. Cell viability plots obtained from MTT assay of complex **1** in MCF-7 cells on light exposure (L, 600-720 nm, 20 min exposure, light dose: 30 J cm^{-2}) and in dark (D) condition.

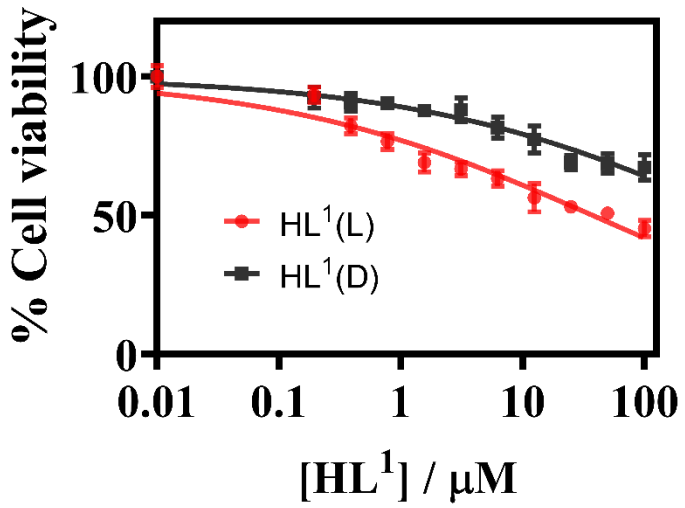

Figure S40. Cell viability plots obtained from MTT assay of **HL^1** in HPL1D cells upon light irradiation (L, 600-720 nm, 20 min exposure, light dose: 30 J cm^{-2}) and in dark (D) condition.

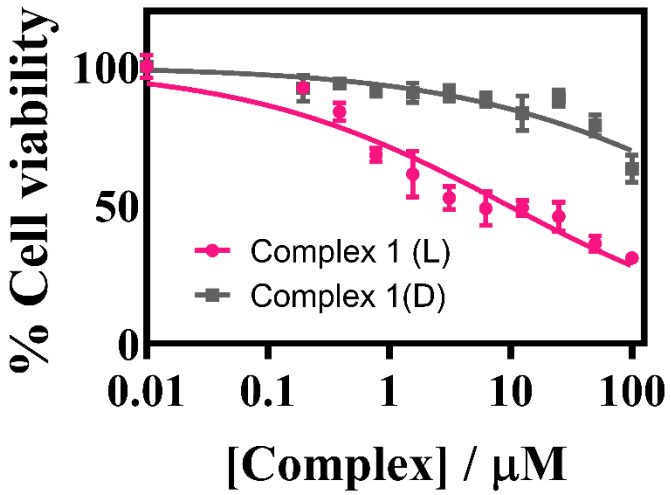

Figure S41. Cell viability plots obtained from MTT assay of complex **1** in HPL1D cells upon light irradiation (L, 600-720 nm, 20 min exposure, light dose: 30 J cm^{-2}) and in dark (D) condition.

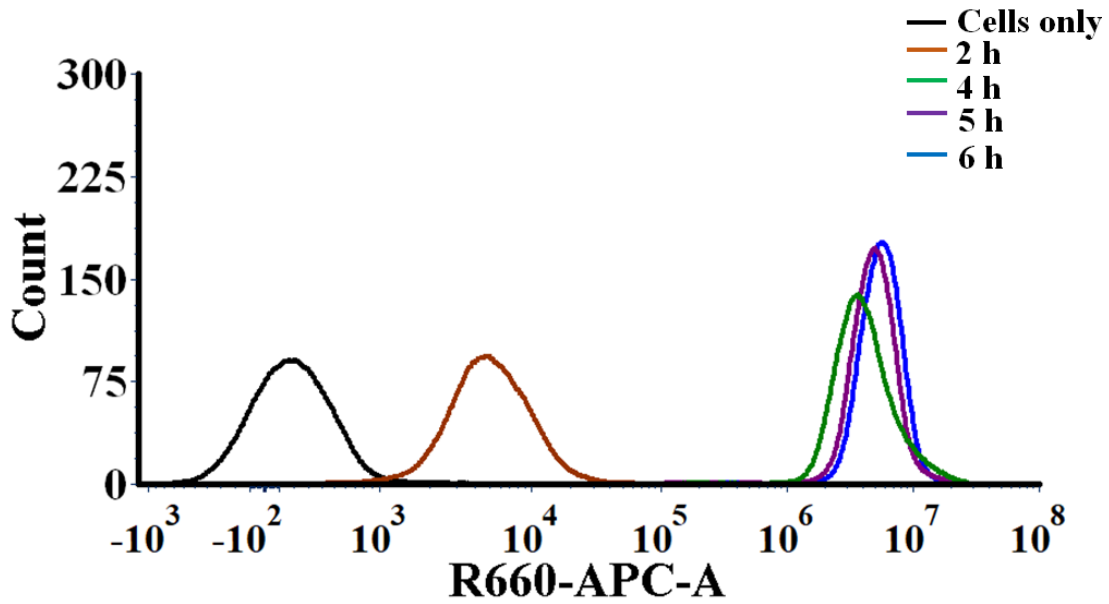

Figure S42. Time-dependent cellular uptake plot of complex **1** in HeLa cells by FACS analysis.

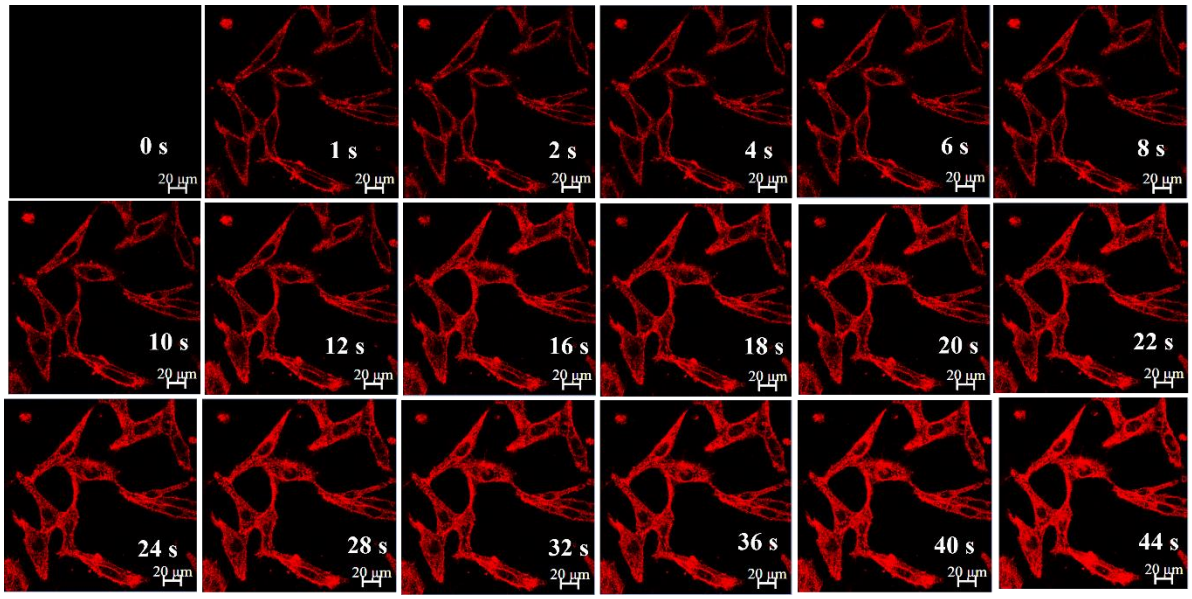

Figure S43. CLSM series images obtained from live cellular uptake of complex **1** (2 μM) in HeLa cells with no time interval with band path of 660 nm to 750 nm by using λ_{ex} of 633 nm. Scale bar: 20 μm.

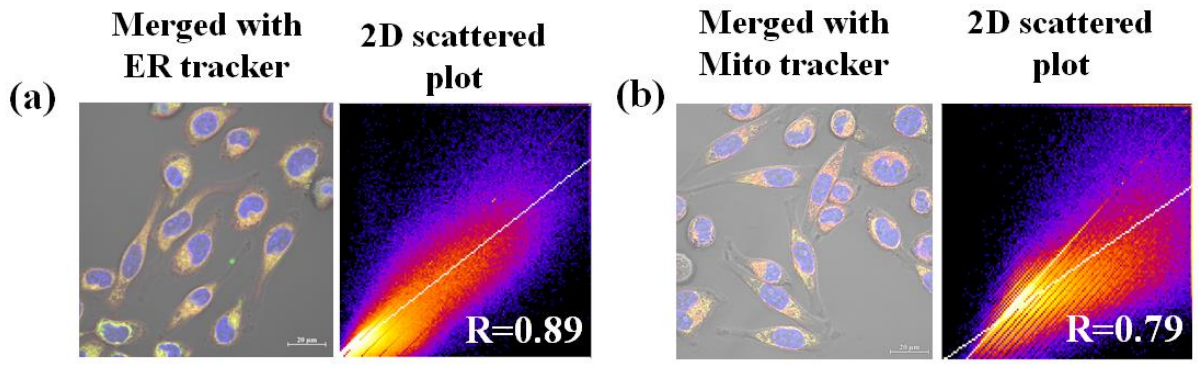

Figure S44. Merged images with emissive trackers along with 2D scattered plot for Pearson's correlation coefficient (PCC) calculations for complex **1**.

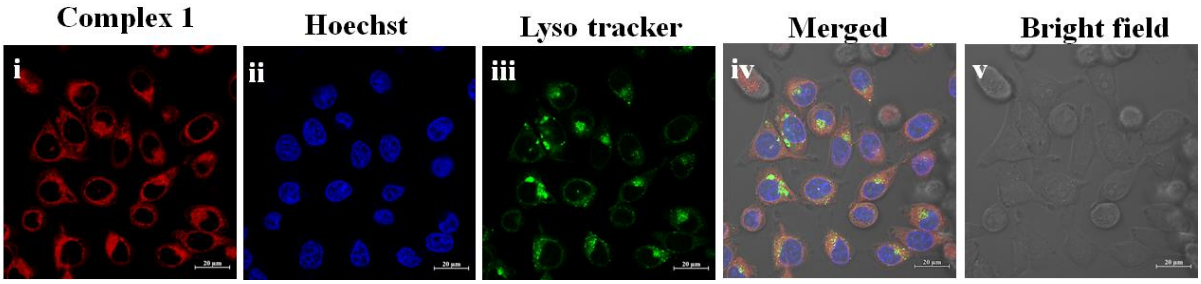

Figure S45. Confocal images for HeLa cells with suitable trackers and complex **1**. Panel (i) shows red emission of complex **1**, panel (ii) shows blue emission of nucleus staining dye Hoechst, panel (iii) shows green emission of Lyso tracker, panel (iv) shows merged image, panel (v) shows bright field.

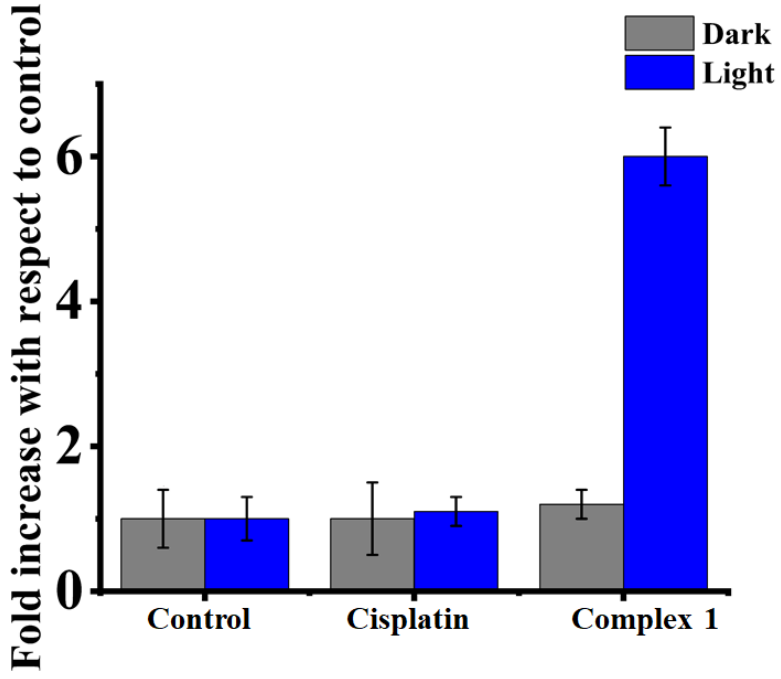

Figure S46. Effect of metal complex on caspase-3/7 activity in HeLa cells upon treatment with 0.5×IC_{50} concentration.

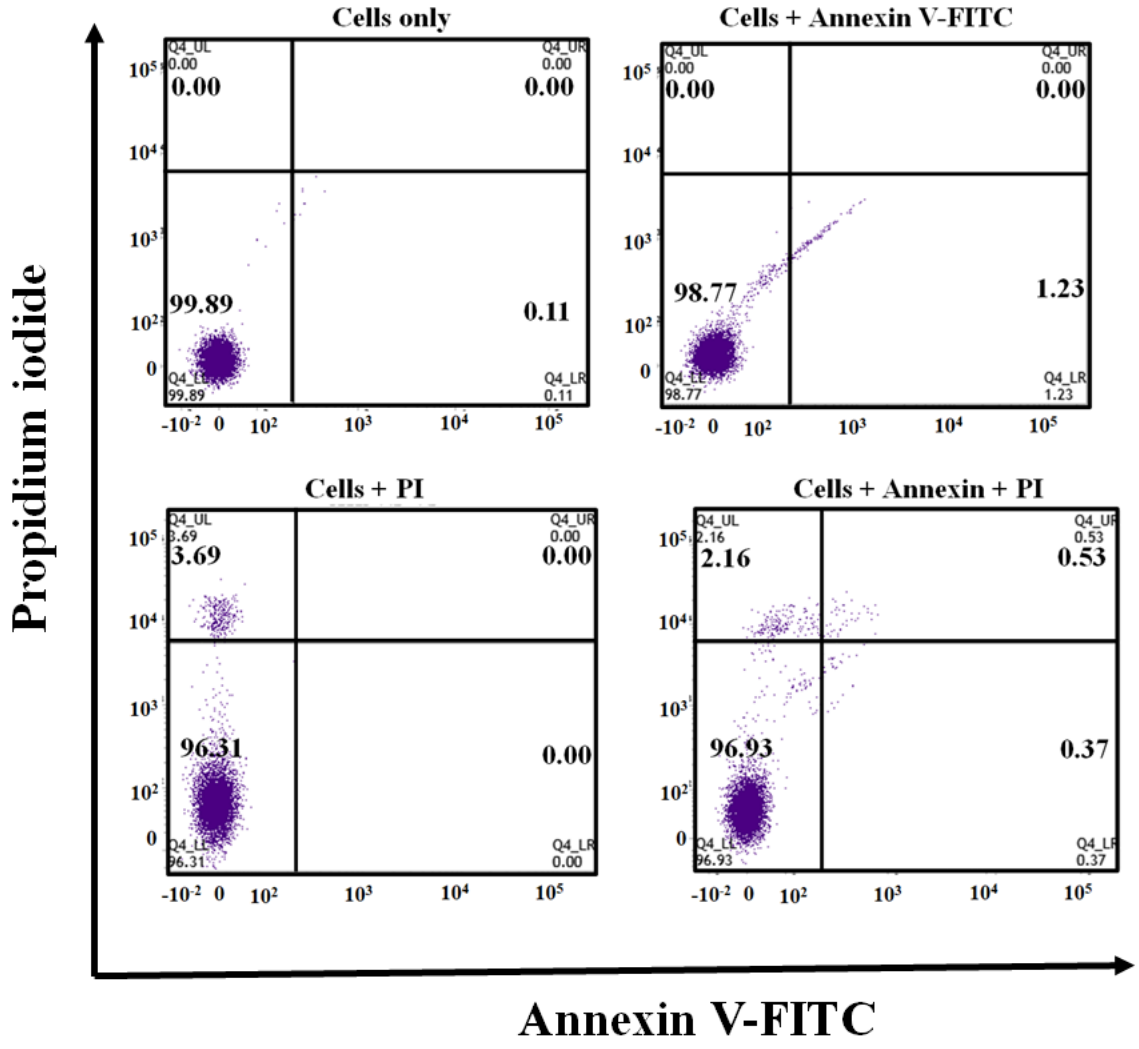

Figure S47. Annexin V-FITC/propidium iodide assay in HeLa cells: (a) cells only; (b) cells + annexin V-FITC (c) cells + propidium iodide; (d) cells + annexin V-FITC + propidium iodide. The %cell population is shown in respective quadrant [lower left: live cells, lower right: early apoptotic cells, upper right: late apoptotic cells, upper left, dead cells]. PI in these plots is propidium iodide.

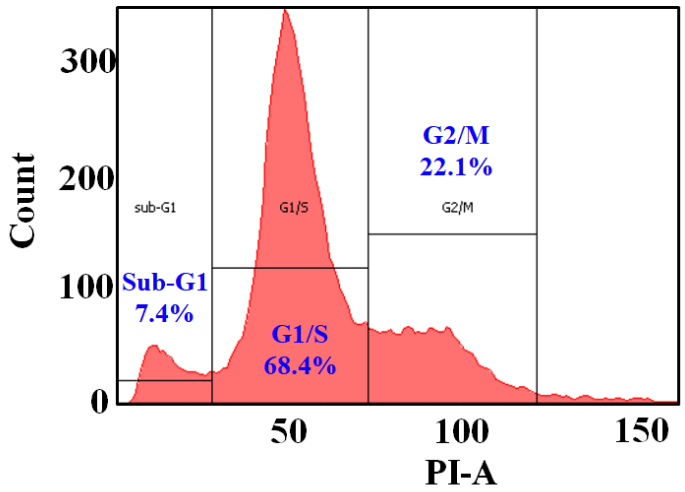

Figure S48. Cell cycle progression in HeLa cells in the control set.

Table S1. Selected physicochemical data for complex **1** and **HL**[1]

Entry	Complex **1**	**HL**[1]
UV-vis: λ_{max}/nm (ε/M^{-1} cm^{-1})[a]	373 (5.74 × 10^4), 598 (3,75 × 10^4) (sh), 650 (8.77 × 10^4)	373 (6.53 × 10^4), 598 (3.95 × 10^4) (sh), 650 (10.99 × 10^4)
Emission: λ_{em}/nm (Φ_F)[b]	674 (0.37)	674 (0.45)
Φ_Δ ($^1O_2$)[c]	0.28	0.16
^{1}H NMR chemical shift (δ, ppm) of γ-proton of BODIPY[d]	6.95	6.95

[a] In 1:1 (v/v) DMSO/DPBS medium. sh, shoulder. [b] Emission wavelength and fluorescence quantum yield (Φ_F). The excitation wavelength (λ_{ex}) = 630 nm. [c] Singlet oxygen quantum yield Φ_Δ in DMSO. [d] In DMSO-d_6.

Table S2. Selected bonding parameters, namely, bond lengths (Å) and bond angles (°) for ligand precursor **Me-L**[1]

Bond lengths	B(1)-N(1)	1.541(4)
	B(1)-F(1)	1.393(4)
	O(1)-C(2)	1.328(3)

	O(2)-C(2)	1.211(4)
Bond angles	N(1)-B(1)-N(2)	106.4(2)
	F(1)-B(1)-F(2)	108.7(3)
	O(1)-C(2)-O(2)	123.7(3)
	O(3)-C(20)-C(21)	115.4(3)

Table S3. Coordinates of optimized geometry for complex **1** obtained from DFT using B3LYP/LanL2DZ level of theory for all atoms

Pt	7.89047600	0.00005500	-0.50366800
N	7.53894500	-1.58174800	-1.84027600
H	7.56668600	-2.41056500	-1.23108300
N	7.53861500	1.58206800	-1.83994200
H	6.63280400	1.50359700	-2.30770600
H	7.56634400	2.41076600	-1.23058400
Cl	8.45566400	-1.78703600	1.01872700
Cl	8.45533500	1.78694000	1.01909200
H	8.34103400	-1.58402100	-2.48021500
O	9.73524800	0.00028800	-1.33342200
O	5.83684600	-0.00012100	-0.22689300
C	5.16609100	-0.00026800	0.96073400
O	5.69522700	-0.00040600	2.08572200
C	3.05165100	-0.00017700	-0.48673900
C	2.86041400	-0.00030700	1.94051800
C	1.65081500	-0.00015000	-0.59523000
H	3.67353800	-0.00014000	-1.37589700
C	1.46109600	-0.00027500	1.83015400
H	3.34967100	-0.00036800	2.91013500
C	0.84193900	-0.00019500	0.56152800
H	1.17893000	-0.00009200	-1.57469600
H	0.84564400	-0.00031100	2.72620300

C	-0.65241700	-0.00014600	0.43646100
C	-1.35099600	-1.22623600	0.37354800
C	-1.35091300	1.22599500	0.37360200
N	-2.75672600	-1.24553000	0.23465800
C	-0.89932900	-2.60075800	0.43975200
N	-2.75664100	1.24538900	0.23470600
C	-0.89915500	2.60048400	0.43987200
C	-3.18790000	-2.55363000	0.21190900
B	-3.63698700	-0.00003800	0.08475100
C	0.50167200	-3.13241400	0.59902400
C	-2.04028600	-3.39893200	0.33904400
C	-3.18772900	2.55351900	0.21201100
C	0.50187900	3.13204100	0.59918300
C	-2.04005900	3.39873800	0.33919000
C	-4.58098700	-2.91316500	0.08322100
F	-4.29984300	0.00000900	-1.20745000
F	-4.69481200	-0.00002000	1.08051200
H	1.16462700	-2.79618000	-0.20666600
H	0.48809500	-4.22801800	0.59213400
H	0.95866400	-2.80754200	1.54114100
H	-2.05622700	-4.47939600	0.35972700
C	-4.58079100	2.91315400	0.08332800
H	0.95884800	2.80707900	1.54128000
H	0.48837000	4.22764700	0.59236400
H	1.16481500	2.79581900	-0.20652700
H	-2.05592900	4.47920200	0.35992500
C	3.66741600	-0.00025200	0.78220700
H	10.43077900	0.00027100	-0.64083300
H	8.34059000	1.58458700	-2.48001800
H	6.63320700	-1.50330600	-2.30818300
C	-5.03228600	-4.20349600	0.04819000
C	-5.03199100	4.20351700	0.04824700

H	-4.30240500	-5.01160100	0.11382100
H	-4.30204800	5.01156900	0.11384400
H	-5.28014600	-2.08625100	0.02002200
H	-5.28000300	2.08629000	0.02006800
C	-6.42464600	-4.63873800	-0.06833300
C	-6.71266400	-6.03133300	-0.09829600
C	-7.51988400	-3.74161800	-0.15054800
C	-8.02154800	-6.50760900	-0.20520800
H	-5.89204300	-6.74374600	-0.03582000
C	-8.83902500	-4.20409400	-0.25745000
H	-7.34506800	-2.66963500	-0.12914700
C	-9.09454400	-5.59399500	-0.28526400
H	-8.24069400	-7.57064100	-0.22777400
H	-9.65094500	-3.48619800	-0.31671100
C	-6.42431900	4.63886200	-0.06826900
C	-6.71223100	6.03147900	-0.09826600
C	-7.51962700	3.74182500	-0.15044800
C	-8.02107900	6.50785200	-0.20518100
H	-5.89155500	6.74383000	-0.03581800
C	-8.83873300	4.20439900	-0.25735100
H	-7.34489300	2.66982900	-0.12901800
C	-9.09414600	5.59431900	-0.28520300
H	-8.24014300	7.57090100	-0.22777600
H	-9.65070900	3.48656400	-0.31658500
O	-10.36276500	6.16211800	-0.38842400
O	-10.36320700	-6.16169900	-0.38847200
C	-11.52280000	-5.28257200	-0.46642900
H	-11.60938200	-4.65885000	0.43395500
H	-11.47685200	-4.64209800	-1.35802900
H	-12.38439100	-5.94924900	-0.53647800
C	-11.52241200	5.28307600	-0.46654900
H	-11.47645700	4.64270200	-1.35822000

H	-11.60908600	4.65925600	0.43375800
H	-12.38395500	5.94981800	-0.53657000

Table S4. Excitation energies and oscillator strengths obtained from TD-DFT calculations for complex **1**

Energy(eV)	λ/nm	Oscillator strength(f)	Transition
1.9483	636	1.0369	HOMO→LUMO+1
2.1520	576	0.0013	HOMO→LUMO+2
2.6349	470	0.0002	HOMO-7→LUMO
2.6722	463	0.4680	HOMO-1→LUMO+1
2.8574	433	0.0001	HOMO-6→LUMO
2.9807	415	0.0001	HOMO-6→LUMO
3.0307	409	0.0001	HOMO-1→LUMO+2
3.0378	408	0.0000	HOMO-2→LUMO

REFERENCES

S1. G. M. Sheldrick, *Acta Crystallogr., Sect. C: Struct. Chem.*, 2015, **C71**, 3−8.

S2. L. J. Farrugia, *J. Appl. Crystallogr.*, 2012, **45**, 849−854.

S3. G. M. Sheldrick, *Acta Crystallogr., Sect. A: Found. Adv*., 2015, **A71**, 3−8.

S4. A. D. Becke, *Phys. Rev. A: At., Mol., Opt. Phys.,* 1988, **38**, 3098-3100.